"Smart" Nanoprobes for Visualization of Tumor Microenvironments

Tiancong Ma, Peisen Zhang, Yi Hou, Haoran Ning, Zihua Wang, Jiayi Huang, and Mingyuan Gao*

Physiological parameters in tumor microenvironments, including hypoxia, low extracellular pH, enzymes, reducing conditions, and so on, are closely associated with the proliferation, angiogenesis, invasion, and metastasis of cancer, and impact the therapeutic administrations. Therefore, monitoring the tumor microenvironment is significant for diagnosing tumors, predicting the invasion potential, evaluating therapeutic efficacy, planning the treatment, and cancer prognostics. Noninvasive molecular imaging technologies combined with novel "smart" nanoparticle-based activatable probes provide a feasible approach to visualize tumor-associated microenvironment factors. This review summarizes recent achievements in the designs of "smart" molecular imaging nanoprobes responding to the tumor microenvironment–related features, and highlights the state of the art in tumor heterogeneity imaging.

1. Introduction

Prognostic factors of malignant tumor, such as growth, invasion, and metastasis, are closely associated with variations in physiological parameters, including hypoxia,[1] low extracellular pH,[2–4] enzyme,[5–7] reducing conditions, etc.[8] For instance, hypoxia is considered to be a common feature in solid tumor microenvironment, which is related to cell behavior changing, extracellular matrix remodeling, and the metastatic behavior increasing.[9–11] The lowered extracellular pH is also deemed to be a hallmark of cancer due to the lactic acid from high aerobic glycolysis,[12] which would induce the cell apoptosis, promote angiogenesis via affecting the concentration of the vascular endothelial growth factor, and enhance invasion through affecting the activity of enzymes.[4,13,14] Therefore, detecting the parameters in tumor microenvironment and clarifying their relationship are significant for diagnosing tumor, predicting the invasion potential, evaluating therapeutic efficacy, planning the treatment, and cancer prognostics.

The tumor-associated microenvironment factors are commonly analyzed in vitro at the molecular level by identifying the characteristic proteins in certain tumor cells and the different gene expressions between tumor and normal tissues.[15,16] However, the in vitro characterizations cannot reveal the spatial heterogeneity of these tumor-associated parameters and their evolution with time. Therefore, the method for analyzing these physiological parameters in vivo is becoming essential.

Most reported in vivo investigations on tumor microenvironment are through invasive methods. For example, in order to detect oxygen or pH in tumor,[17–22] microelectrodes are inserted into accessible tumors, such as cervix, prostate, head, and neck. Although they are accurate, these invasive methods are unable to provide the information of the entire tumor region because only one value of a location can be obtained at one time.

In comparison with invasive methods, noninvasive molecular imaging with the aid of delicate imaging probes can provide spatiotemporal information of cellular or even molecular level biological process.[23–29] The probes have been designed to target at the certain cell or proteins and produce signal which can be received and analyzed. Tumor-associated microenvironment physiological parameters are important hallmarks, rendering them attractive targets when designing bioresponsive "smart" nanoprobes.[30] Thus, well designing upon novel chemistries is significant to construct ultrasensitive target-triggering probes for success of noninvasive molecular imaging in vivo.

A series of molecular imaging probes have emerged, including small molecular probes,[31] biomolecular probes,[32] nanoparticle (NP)-based probes,[33–38] etc. NP provides an ideal platform for developing novel probes, especially for tumor microenvironment imaging.[39] NPs with regular size tend to accumulate in tumor region instead of normal tissue due to the newly formed leaky vessels and poor lymphatic drainage, which is referred to the enhanced permeation and retention (EPR) effect.[40,41] In addition, NPs provide an ideal platform for loading tumor-targeting molecules, such as tumor specific monoclonal antibody, and for designing activatable "smart"

T. C. Ma, P. S. Zhang, Prof. Y. Hou, H. R. Ning, Dr. Z. H. Wang, J. Y. Huang, Prof. M. Y. Gao
Key Laboratory of Colloid
Interface and Chemical Thermodynamics
CAS Research/Education Center for Excellence in Molecular Sciences
Institute of Chemistry
Chinese Academy of Sciences
Bei Yi Jie 2, Zhong Guan Cun, Beijing 100190, China
E-mail: houyi@iccas.ac.cn
T. C. Ma, P. S. Zhang, H. R. Ning, J. Y. Huang, Prof. M. Y. Gao
School of Chemistry and Chemical Engineering
University of Chinese Academy of Sciences
Beijing 100049, P. R. China
The ORCID identification number(s) for the author(s) of this article can be found under https://doi.org/10.1002/adhm.201800391.

DOI: 10.1002/adhm.201800391

probes which can respond to stimuli in tumor microenvironment through novel surface engineering. The smart nanoprobes can be designed to sensitively produce signals at the target region, and provide information of the physiological parameters in tumor microenvironment, which is helpful for generating images of the anatomical structures of living organs with high resolution and real-time quantitative detection of the certain biomarkers. Thus, the responsive molecular imaging nanoprobes show limitless prospect in studying biological process and analyzing diseases directly in vivo.[42,43] In the current review, we will summarize the preparation strategies, response mechanisms, and biological applications of activatable optical imaging nanoprobes, magnetic resonance (MR) imaging nanoprobes, and photoacoustic (PA) imaging nanoprobes (**Figure 1**).

Optical imaging is a method that generates the images based on the detecting of the photons from fluorescent or luminescent probes in target region. Among activatable molecular imaging nanoprobes, optical imaging nanoprobes seem to attract the most attention from researchers due to the real-time feedback of this imaging modality, the rapid change of optical materials under various stimuli, and the excellent quenching ability of certain nanoparticles including gold nanoparticles,[44] iron oxide nanoparticles,[45] and so on. Fluorescence imaging is one of the most potential optical imaging. After excitation of the fluorescence nanoprobes, the signal can be observed directly by the naked eye, camera systems, or optical microscopy at higher resolution.[46–48] Besides, the large anti-Stokes upconversion luminescent (UCL) process owned by rare earth upconversion luminescent nanoparticles (UCNPs) avoids the photodamage to organisms, reduces the background autofluorescence, and greatly improves tissue penetration depth of excitation light. These fascinating characters enable UCNPs as promising platform to design activatable optical imaging nanoprobes.[35,49–56]

MR imaging is a common imaging technique in clinical tumor diagnosis, which is based on imaging of the relaxation signals of water proton spins. It has been demonstrated as a powerful tool due to its cellular and even subcellular spatial resolutions for anatomical structure imaging.[36,37] However, due to unsatisfied sensitivity, enhancing the contrast between the malignant tumor and normal tissues remains a big challenge. In recent years, various nanoprobes,[57–65] especially activatable magnetic resonance imaging (MRI) nanoprobes,[57,66–68] were designed to enhance the sensitivity. Thus, it is covered in this review.

PA imaging is a newly emerged imaging modality that relies on the photoacoustic effect. Combining optical and ultrasound imaging techniques, this imaging modality shows better tissue penetration ability and improved spatial resolution in vivo.[69,70] A series of responsive PA imaging probes are reported for the detection of tumor microenvironment under the stimuli of pH or enzyme.[71–73] Thus, we also summarize the development of the smart PA imaging nanoprobes.

2. Activatable Optical Imaging Nanoprobes

To design successful activatable optical imaging probes, the optical properties of materials and the adopted activatable principle are both needed to be elaborated. Among the various designs that have been reported recently, anyway, an overwhelming majority of responsive optical imaging probes can be summarized as "turn-on" type. The "turn-on" type, in other words, "off–on" type implies that signal in responsive probes is quenched and can be activated to the fluorescent state. Besides the nanoprobes turned on by single stimulus, the novel multiresponsive type optical imaging nanoprobes have been reported by pioneers and our group. Therefore, these types of

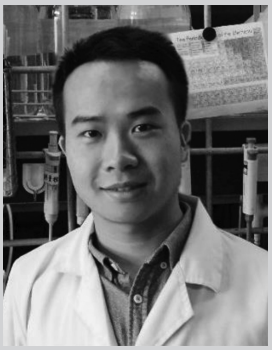

Tiancong Ma received a B.S. degree in polymer materials science and engineering in 2013 at the South China University of Technology. He is currently a Ph.D. student in the Institute of Chemistry, Chinese Academy of Sciences supervised by Prof. Mingyuan Gao. His research interests include synthesis and applications of inorganic functional nanomaterials.

Yi Hou is an Associated Professor in the Institute of Chemistry, Chinese Academy of Sciences. He received his B.S. (2000) and Ph.D. (2009) in physical chemistry at the University of Science and Technology of China. He worked as a Postdoctoral fellow in the University of Toronto from 2010 to 2011. He took his current position in 2011. His major research focuses on synthesis and bioapplications of functional nanomaterials.

Mingyuan Gao is a Full Professor in the Institute of Chemistry, Chinese Academy of Sciences. He received his B.S. (1989) and Ph.D. (1995) in polymer chemistry and physics at the Jilin University. He worked as a research assistant and associate in Germany from 1996 to 2002 and was an A. v. Humboldt fellow between 1996 and 1998. He took his current position upon a "Hundred-talent Program" of the CAS in 2001. He received the "National Science Fund for Distinguished Young Scholars" from the NSFC in 2002. His research focuses on the synthesis as well as biological and biomedical applications of functional nanomaterials.

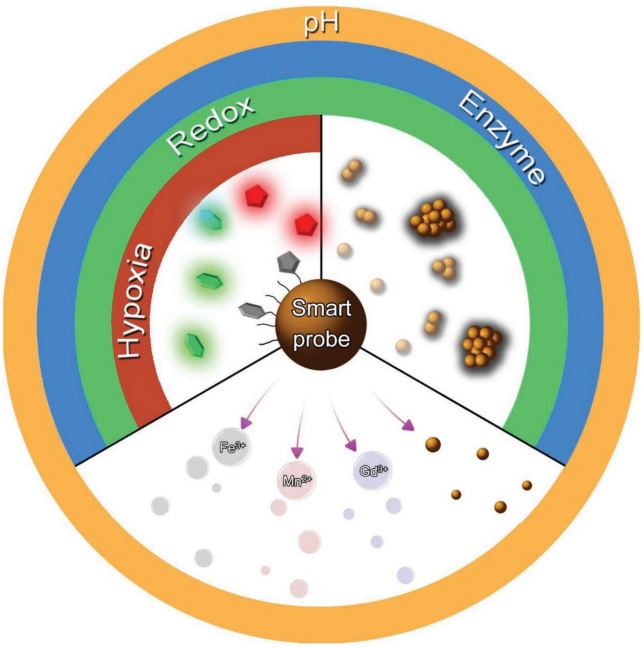

Figure 1. Illustration of stimuli-responsive mechanism of smart nanoprobes within different tumor microenvironment parameters. The low pH induced by high level of anaerobic glycolysis could serve as a trigger to release optical or magnetic elements, or self-assemble, leading to activated optical, MR, and PA imaging. The parameters including unusual redox conditions, tumor-associated enzymes, and hypoxia, can be used to design probes, in which the linkers would be cut off to release optical molecules in tumor tissues. Activated MRI tumor nanoprobes based on nanoparticle aggregation triggered by redox species and proteases have also been developed.

responsive optical nanoprobes are concluded in this part, and in each section, activatable nanoprobes according to different stimuli are included.

2.1. Single Stimuli–Responsive "Turn-On" Type Nanoprobes

To target the single tumor-associated microenvironment biomarker, an ideal "off–on" type responsive optical probe should be almost nonemission in the blood or normal tissue microenvironment while highly luminous in tumor microenvironment. There are several quenching mechanisms for designing activatable optical imaging nanoprobe, including fluorescence resonance energy transfer (FRET), photon-induced electron transfer (PeT), charge transfer, and H-dimer formation. The FRET effect, the mechanism describing energy transfer from donor to acceptor, is the most widely used mechanism for activatable fluorescence probes and almost available in all stimuli. In addition, ratiometric type responsive optical probes are also discussed in the following sections.

2.1.1. O_2-Sensitive Nanoprobes

As a tumor grows, the rapid proliferative cancer cells will become far beyond oxygen (O_2) delivery from tumor vasculature, resulting in the intratumor regions having a significantly lower oxygen concentration than healthy tissues. Thus, hypoxia is a common feature in tumor microenvironment.[74–76] For hypoxia imaging, nitroaromatic, azobenzene derivatives, polypyridyl, and pyrenyl units are widely applied to design responsive probe due to their relatively high sensitive conversion under hypoxic conditions. As an example, azobenzene, which will degrade in hypoxic environment, is widely used in responsive hypoxia imaging as bioreductive linker, and has been reported in targeted small interfering ribonucleic acid (siRNA) delivery.[77] To improve the sensitivity and specificity for in vivo imaging, oxygen-sensitive groups instead of hypoxia-responsive groups, were considered to fabricate smart nanoprobes, such as transition metal complexes.[78,79]

Zheng et al. achieved ultrasensitive detecting of tumor or even a tiny amount of tumor cells via developing an oxygen-sensitive, near-infrared optical imaging probe in 2015.[79] The iridium (III) complex, containing a large conjugated ligand, is the key functional components of this complex probe (Ir–poly(*N*-vinylpyrrolidone) (PVP)). This complex can be quenched by O_2 in normal tissues and emit light in near-infrared (NIR) region in tumor microenvironment due to the low O_2 concentration. The phosphorescence emission at 710 nm endows the probe light penetration for deep-tissue imaging. They developed nanoprobes based on the same O_2-sensitive chromophore.[80] The nanoprobe is the micelle prepared by the Ir–PVP and poly(e-caprolactone)-*b*-poly(*N*-vinylpyrrolidone) (PCL–PVP). The O_2-sensitive chromophore and the PCL block form the core due to their hydrophobicity, while the PVP chains constitute the shell because of their hydrophilicity and biocompatibility. The performance of this activated nanoprobe was evaluated in various animal models. The results demonstrated that, this hypoxia-activated optical imaging nanoprobe successfully obtained the 60-fold stronger phosphorescent signal in metastases-bearing lung than that in normal tissue 48 h after injection. In addition, 30-fold stronger signals from lymph nodes in metastases-bearing mice comparing with that from normal mice 1 h after injection were also detected.

Semiconductor nanocrystals have also been reported to design quantum dot (QD)–dye oxygen sensor due to their excellent optical properties.[81] Based on ratiometry between oxygen indicator and the QDs, Amelia et al. reported an oxygen-responsive luminescent nanosensor with high dynamic range.[82] The CdSe@ZnS QDs' surface was modified by O_2-sensitive chromophore, pyrenyl units, through chemical adsorption. The emission of QDs is quite stable under the aerobic condition, while pyrenyl units are strongly quenched by O_2. Thus, ratiometric response between these two emissions can be used to measure O_2 pressure. Though these QDs are strongly hydrophobic and need further modified for sensing in vivo, the probe function can measure a dynamic range from 0 to 1.013 bar O_2.

For in vivo imaging, lanthanide-doped UCNPs have attracted great attention and have been applied as a platform to fabricate activatable probe, because of the unusual upconversion optical properties correlated with f-electrons. Liu et al.[83] prepared an O_2-sensitive nanoprobe by encapsulating $[Ru(dpp)_3]^{2+}Cl_2$, oxygen indicator, into the hollow space of UCNP@hollow mesoporous SiO_2 ($mSiO_2$) (**Figure 2**). The luminescence of $[Ru(dpp)_3]^{2+}Cl_2$ at 613 will be quenched in the presence of oxygen. Upon 980 nm excitation, the upconversion

luminescent emissions of $NaYF_4$:Yb,Tm@$NaYF_4$ UCNPs at 450 and 475 nm can excite $[Ru(dpp)_3]^{2+}Cl_2$ and form the luminescence resonance energy transfer system. The reversible luminescent quenching and recovery of nanoprobe dependent upon O_2 concentration were observed in zebrafish embryos' brain via confocal laser scanning microscopy for several times. The results demonstrated that the nanoprobe based on UCNP platform and oxygen indicator can be a powerful tool to achieve hypoxia detection in vivo.

2.1.2. pH-Sensitive Nanoprobes

Acidic extracellular fluid caused by the significantly enhanced aerobic glycolysis, is a universal phenomenon of solid tumors and a critical signature of carcinoma. The extracellular pH (pH_e) of normal tissues is kept constant in a range of 7.2–7.4. However, in most tumors, pH_e is typically lower than that of normal tissue and range in 6.2–6.9. Thus, designing pH-sensitive nanoprobes is promising in monitoring tumor and tumor microenvironment. A large amount of pH-sensitive optical probes have already been prepared. The typical pH-sensitivity mechanisms include the protonation of ionizable groups, the degradation of acid-cleavable bonds, and so on.

pH change can induce certain groups charge variation, which further induces the conformational transition. Based on this responsive action, Chiu et al. reported a pH-sensitive nanoprobe composed by associating polyelectrolyte, *N*-palmitoyl chitosan (NPCS).[84] The NPCS bearing the donor (Cy3) or the acceptor (Cy5) moiety was first completely mixed in the aqueous solution and forms nanoscale network clusters at pH 4.0. Under acidic conditions, the charge repulsion among the protonated amine groups results in the expanding of NPCS chains in nanoscale network. In this state, the distance between donor (Cy3) and acceptor (Cy5) will lie within the suitable range for FRET and the energy transfer will take place. On the contrast, higher pH can result in the deprotonation of the amine groups and the increase in hydrophobicity of NPCS. The distance between Cy3 and Cy5 moieties will be too far to achieve energy transfer. Hence, pH-sensitive FRET system induced by the conformational transition has successfully mapped spatial pH changes in the biological microenvironment.

pH change can also induce the degradation of pH-sensitive materials. According to this mechanism, pH-activatable nanoprobes have been constructed based on energy transfer between fluorophores in aggregates, which can be dissolved at low pH. Li et al. designed a pH-sensitive NIR nanoprobe relying on intramolecular energy transfer of IR783 in self-assembling poly(L-lysine) (PLL) conjugated with dextran.[85] The self-quenching NIR fluorophore IR783, labeled in the polymer via pH labile hydrazone bonds, keeps an "off" state in normal tissue due to nonradioactive decay. While, the fluorescence will recover in the acidic tumor microenvironment because of the cleavage of fluorophores from the nanoprobes. The in vivo imaging suggested that the NIR fluorescence of IR783 in acidic tumor microenvironment increased 4.3 times at 24 h after injection of nanoprobes, providing a design strategy of pH-activated NIR nanoprobes for noninvasively visualizing tumors in vivo.

Similarly, Zhou et al. designed a series of tunable, pH-activatable micelle nanoparticles (pHAMs) using an ionizable block copolymer design. They first synthesized copolymers (PEO-*b*-PR) with ionizable tertiary amine block (PR) and poly(ethylene oxide) (PEO) segments.[86] At high pH, the neutralized PR segments self-assemble into the micelles due to the increasing hydrophobicity, which results in fluorescence quenching through the mechanisms of FRET and PeT. In low pH environment, micelles disassembled because of protonated PR segments, and fluorophores emitted strong fluorescence. The pK_a values of ammonium groups and PR hydrophobicity can be adjusted to render different pH transitions. These ultra-pH-sensitive (UPS) nanoprobes have fast temporal response (<5 ms), sharp pH transitions (< 0.25 pH unit), and high emission intensity ratio between ON/OFF states (up to 55 times). Based on previous strategy to fine-tune the hydrophobicity of the PR segment, the same group expand the UPS design to a library with operator-predetermined pH transitions covering the entire physiologic pH (4–7.4) and wide fluorescent emissions (400–820 nm).[87] There are 10 nanoprobes with 0.3 pH increment in this library which contain different fluorophores, respectively, and each nanoprobe maintained exquisite sensitivity to the environmental pH. The different nanoprobes in the library can be applied in detecting lysosomal pH, monitoring acidic tumor microenvironment pH, studying the maturation of endosomes, and so on. For example, extracellular ultra-pH-sensitive (UPS_e) nanoprobes with a sharp pH transition at 6.9 were synthesized and achieved in vivo tumor imaging in a wide variety of mouse cancer models in 2014.[88] UPS_e nanoprobes were stable and kept silent fluorescence signals in blood pH as self-assembled micelles. However, the fluorescence intensity of nanoprobes was dramatically increased after being activated in acidic A549 tumor microenvironment with large organ to blood ratio (OBR, 355). This approach further achieves the pH-sensitive detection of tumor tissues in 10 different tumor models, suggesting that it seems to be a universal strategy.

2.1.3. Enzyme-Sensitive Nanoprobes

The typical design of enzyme-sensitive nanoprobes is based on certain substrate linkers which can be cleavaged by targeted enzyme. Hydrolysis of ester bond is the widely used mechanism for designing probes to targeting tumor-associated esterases, including phosphatases, intracellular acid hydrolases, and so on. Although the amide bond is more stable than ester bond under chemical conditions in physiological environment, peptide sequences that are vulnerable to cleavage by certain enzymes have been applied for designing activatable probes to hydrolytic protease detections, such as fibroblast activation protein alpha. Azo structures are easily cleaved under reduction condition, so probes containing aromatic azo linkers can be activated by azoreductase enzymes, for hepatic cancer imaging.

Weissleder and co-workers first reported a method for in vivo imaging tumors and quantifying the activity of proteases in tumor cells.[89] A cathepsin B-sensitive peptide was used as the linker to couple the near-infrared-fluorescence (NIRF) dye Cy5.5 to a cross-linked iron oxide (CLIO). In the similar way, a linker of proteolytically resistant L-arginyl residues was used

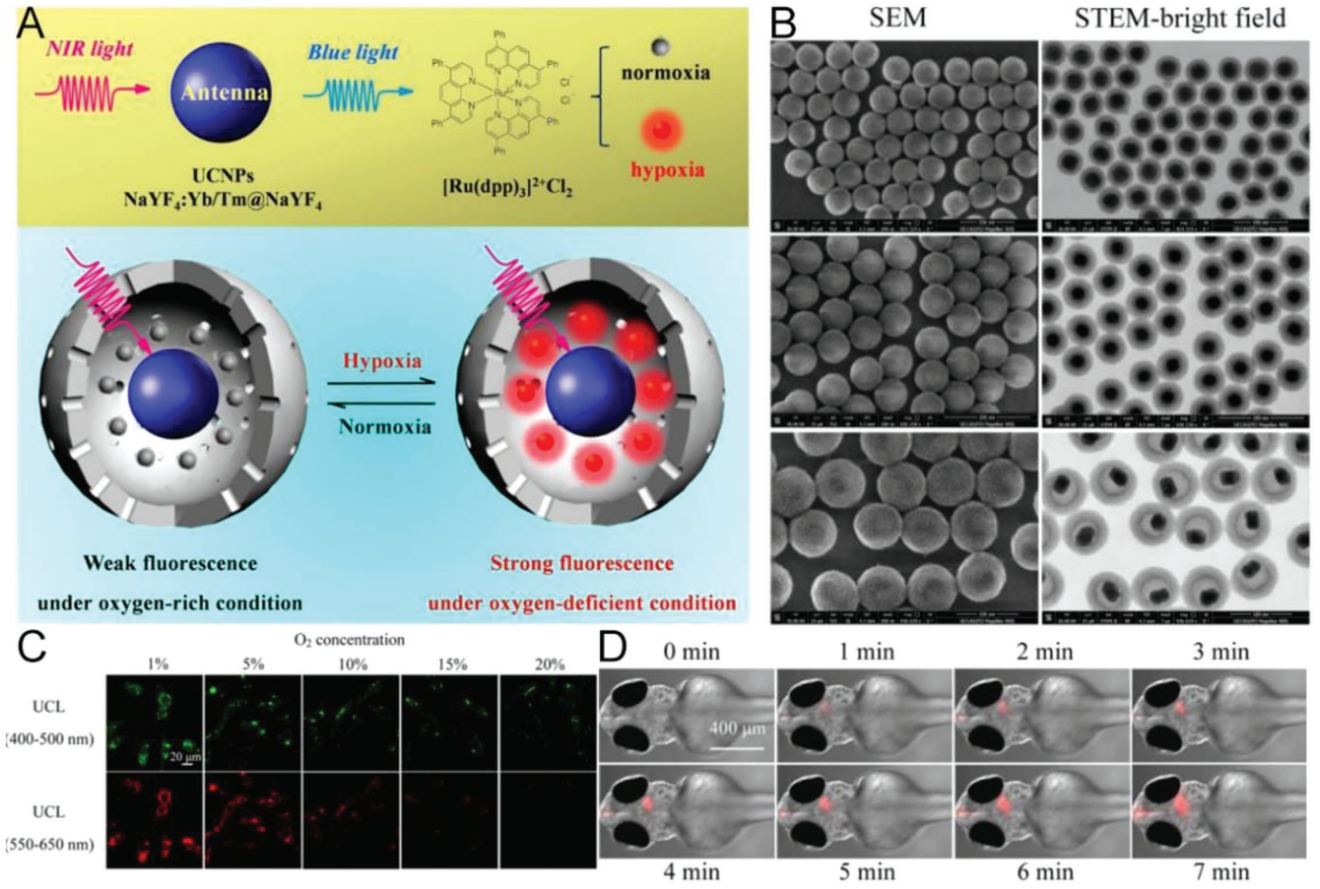

Figure 2. A) Illustration of the nanoprobe structure and the mechanism of O_2-sensitive luminescence. B) Scanning electron microscopy and bright field scanning transmission electron microscopy images of UCNP@dense SiO_2 and UCNP@dense SiO_2@mesoporous SiO_2. C) O_2-sensitive UCL attenuation of nanoprobes incubated with U87MG cells. D) Confocal laser scanning microscopy images of zebrafish embryos after injection of nanoprobes followed by adding 2,3-butanedione. Reproduced with permission.[83] Copyright 2014, American Chemical Society.

to couple the dye Cy3.5 to CLIO. The Cy5.5 fluorescence will increase because of the cleavage of the linker, while the Cy3.5 fluorescence remains constant. In other words, Cy5.5 fluorescence provides information on enzyme activity and Cy3.5 fluorescence reflects the nanoprobes concentration. After mixing these two conjugates, the ratio between Cy5.5 and Cy3.5 can quantitatively monitor the enzyme activity in vivo, independent of the amount of nanoprobes. This research demonstrates that attaching the fluorochrome to the quencher through the smart surface engineer is a successful stratagem for imaging specific enzymes in vivo.

Matrix metalloproteinases (MMPs) are proteolytic enzymes which regulate various tumor cell behaviors including proliferation, apoptosis, invasion, and metastasis.[90,91] As a result, the overexpression of MMPs within the tumor microenvironment can serve as site-specific biomarkers for designing enzyme-sensitive imaging nanoprobes. Conjugating the dye and the quencher with a MMP-cleavable peptide is a wide method to form the turn-on type of probes. Lin et al. chose an energy pair, Cy5.5 and black hole quencher (BHQ, a quencher of Cy5.5 that is widely utilized), to build MMP-sensitive nanoprobes.[92] Cy5.5 was first labeled with peptide (Cy5.5-Gly-Pro-Leu-Gly-Val-Arg-Gly-Cys), a sequence that can be cleaved by several types of MMPs. The dye and quencher were then coupled with ferritins, respectively. Finally, the ferritins labeled by Cy5.5 and quencher would aggregate to form assemblies under neutral pH. In vivo imaging on xenograft tumor demonstrated that the nanoprobes can be activated instantly after exposing to a MMP-rich microenvironment, due to the cleavage of Pro-Leu-Gly-Val-Arg (PLGVR) substrate and the release of Cy5.5.

Biocompatible Au nanoparticles (AuNPs) are commonly used as ultraefficient quencher in activatable imaging probes due to their excellent NIRF quenching properties. Lee et al. described a protease-sensitive near-infrared fluorescence–quenched probe, as shown in **Figure 3**.[93] The AuNPs (20 nm) and Cy5.5 were conjugated with a specific substrate peptide for MMP, that is, Gly-Pro-Leu-Gly-Val-Arg-Gly-Cys. The quenched NIRF signal of this typical AuNP-based enzyme-sensitive nanoprobes will recover in tumor microenvironment. Probes were evaluated in animal model and achieved visual detection of the activities of MMP. Furthermore, this stratagem can be applied to many other proteases in tumor microenvironment by altering the specific substrate linker.

Caspase, a family of protease enzymes associated with cell death, is an ideal biomarker for imaging tumor apoptosis. Designing caspase-sensitive nanoprobes for monitoring

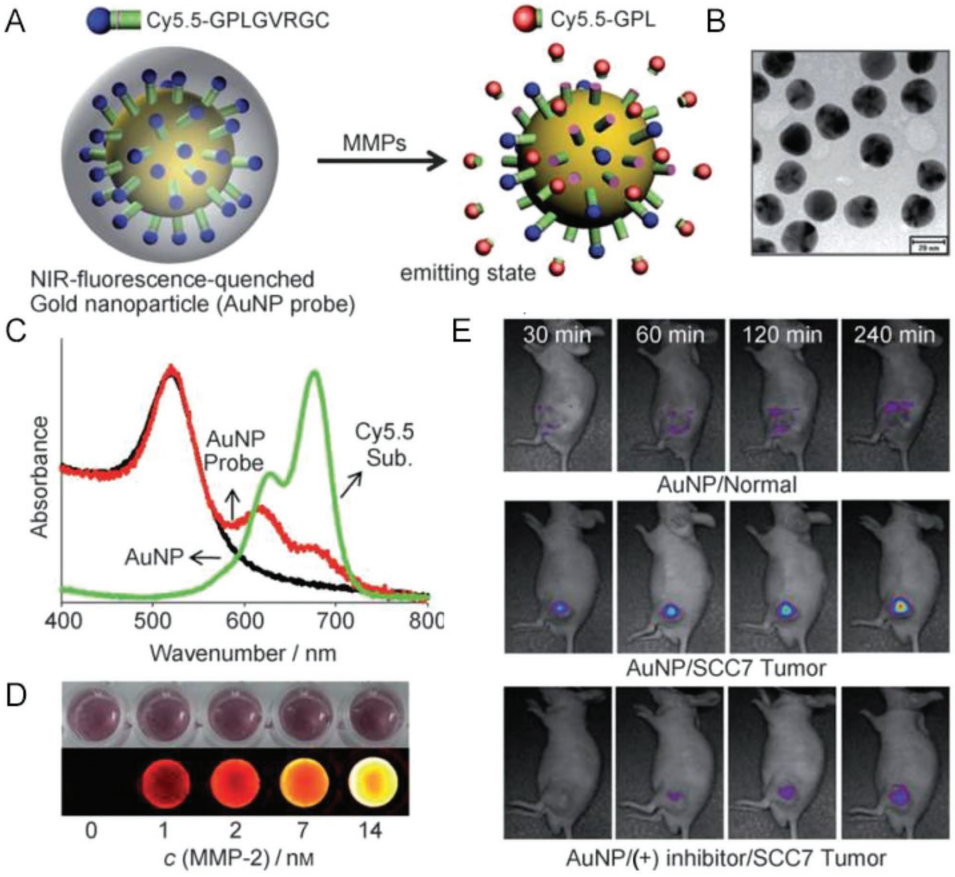

Figure 3. A) The illustration of enzyme-triggered nanoprobe. B) Transmission electron microscopy (TEM) image of the nanoprobe. C) Ultraviolet–visible spectra of AuNP, nanoprobe, and Cy5.5–substrate solutions. D) Corresponding bright and NIRF image sections of a 96-well microplate of the AuNP probes containing various MMP-2 concentrations. E) NIRF tomographic images of normal mice, subcutaneous SCC7 tumor–bearing mice, and subcutaneous SCC7 tumor–bearing mice with inhibitor after injection of the AuNP probe (blue: low intensity, red: high intensity). Reproduced with permission.[93] Copyright 2008, Wiley-VCH.

apoptosis in tumor microenvironment will be greatly helpful in evaluating therapeutic efficacy and anticancer drug delivery. Ye et al. designed a caspase-3/7-sensitive nanoaggregation fluorescent probe (C-SNAF) with NIR fluorescence spectrum, as shown in **Figure 4**.[94] In therapy-responsive tumor microenvironment, increased caspase-3/7 cut the L-Asp-Glu-Val-Asp peptide, leading to the increase in hydrophobicity and the aggregation of the probes. Because these nanoaggregations tend to retain in apoptotic microenvironment, the probes can evaluate tumor response in vivo after therapy by comparing fluorescence intensity in tumor region.

2.1.4. Redox-Sensitive Nanoprobes

The redox conditions are central to various biochemical processes for human beings. For instance, the thiol-containing biomolecules, such as cysteine (Cys) and glutathione (GSH), are important antioxidants in animal cells. It has been indicated that the reductive GSH concentration in tumor tissue is much higher than that in healthy tissues. Additionally, the reactive oxygen species (ROS) such as hydrogen peroxide (H_2O_2), are also found at high levels in most types of solid tumors. Thus, tumor-associated redox species are also alternative targets to design responsive probes.

Based on dithiobis(succinimidyl propionate) (DSP), a linker with the disulfide bond which can be cleaved in reducing conditions, Niko et al. developed a redox-sensitive fluorescencent imaging probe, in which the fluorescent dye NR12D molecules aggregate into micelles due to hydrophobic interaction, and their fluorescences are quenched.[95] The responsive linkers are polymerized to the micelles through conjugation with amino group of NR12D. The fluorescence of the probe can be dramatically increased in cellular reductive environment, because the DSP linkers would be degraded, and the NR12D micelles would be released and fused into membrane. Based on an organic chromophore IR1061 whose NIR absorption can be changed by •OH, generated by H_2O_2 in presence of the Fenton catalysis of Fe^{2+}, Liu and co-workers developed a H_2O_2-sensitive fluorescence imaging probe by using second near-infrared window upconversion nanoparticles.[96] The $NaErF_4$:Ho@$NaYF_4$ nanoparticles show upconversion emission peaks at 980 and 1180 nm under excitation of 1530 nm. Combining with the IR1061, which can effectively quench the fluorescence at

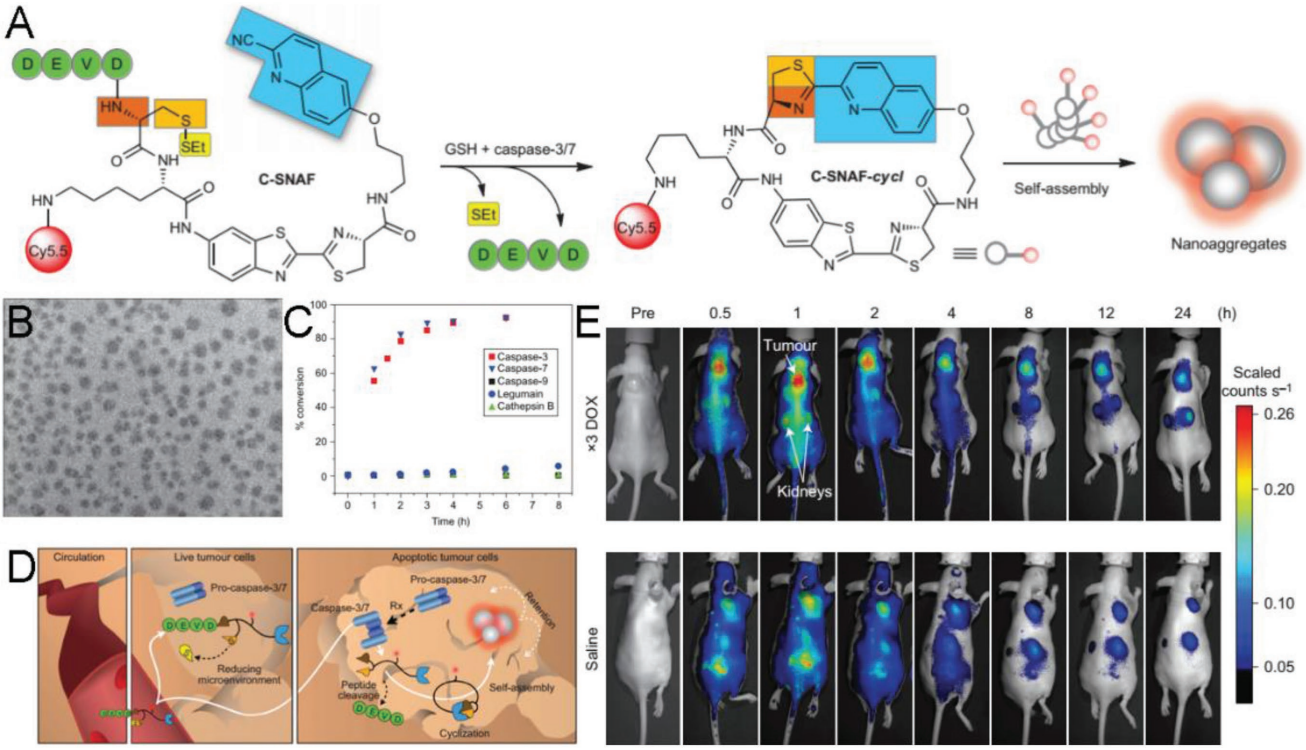

Figure 4. A) Illustration of the structure of caspase-3/7-sensitive nanoprobes and the mechanism of cyclization reaction. B) TEM image of nanoaggregates after incubated with recombinant human caspase-3. C) The studies of enzymatic reaction kinetics and specificity. D) Illustration of the behavior of C-SNAF in vivo. E) Longitudinal fluorescent imaging of ×3 DOX or saline-treated tumor-bearing mice after injection of C-SNAF. Reproduced with permission.[94] Copyright 2014, Springer Nature.

980 nm in absence of H_2O_2, the fluorescence imaging probe can reveal the concentration of H_2O_2 by the ratiometric fluorescence (I_{980}/I_{1180}).

2.2. Multiresponsive Type Nanoprobes

Such above probes are typically responsive to a single biological condition, but the progression of tumor is always the result of multibiological factors. And, these physiological parameters in tumor microenvironment are strongly correlated.[97–102] Therefore, the strategies which rely on multi-biomarkers are developed in recent years. Considering that some acidic materials may potentially pose the tissue of nonspecific activation and cause, Zhao et al. reported MMPs/pH dual-stimuli synergistically and reversibly activatable multifunctional nanoprobes for tumor specific imaging in vivo.[103] They used gold nanorods (AuNRs) as ultraefficient quencher and a pH-activated NIR asymmetric cyanine dye to build the probe. Asymmetric cyanine serves as the tumor-specific imaging probe due to its reversible pH-responsive near-infrared absorption and fluorescence. Meanwhile, a MMP-sensitive peptide sequence (H_2N−GPLGVRGC−SH) was used as the linker to couple the AuNRs and the asymmetric cyanine. The probe only lighted up with MMP-13 in acidic microenvironment, which enables it for tumor-specific imaging and no "false positive" result.

To reveal the correlation among the tumor-associated factors, Hou et al. proposed a protease-activated pH-sensitive ratiometric optical imaging nanoprobe.[45] A MMP-9-sensitive peptide served as the linker to conjugate the ratiometric fluorescent dye, *N*-carboxyhexyl derivative of 3-amino-1,2,4-triazole-fused 1,8-naphthalimide (ANNA), to Fe_3O_4 nanocrystals, as shown in **Figure 5**. The Fe_3O_4 nanoparticle is an ideal quencher for this ratiometric dye. After the cleavage of the peptide in MMP-rich microenvironment, the fluorescence of dye will recover, namely the "on-state." This strategy makes the nanoprobe significantly different from previous sensitive nanoprobes. MMP-9 responsibility reduced nonspecific background, while ratiometric fluorescence can mitigate the negative effects of fluorophore concentration and tissue depth on fluorescence intensity, and allow quantitative determination.[104] In vivo imaging of the pH in tumor region demonstrates the feasibility of this protease-activated pH-sensitive design for microenvironmental pH analysis.

On this basis, Ma et al. extend the concept by adding the NIR fluorescent dye Cy5.5 as the internal reference (**Figure 6**). The constant emission of this internal reference and the fluorescence of MMP-activated pH-sensitive ratiometric dye (ANNA) can form another ratiometric fluorescent system to quantitatively map activity of MMP-9 in tumor microenvironment.[42] In vivo imaging experiments demonstrated that folic acid (FA), with a lower molecular weight than monoclonal antibody, makes the current nanoprobes a more desirable for systemic delivery and the MMP-9 activity is strongly associated with pH in location. For deeply understanding the relationship between pH and MMP-9, tumor microenvironmental pH was adjusted via intratumoral injections of phosphate-buffered

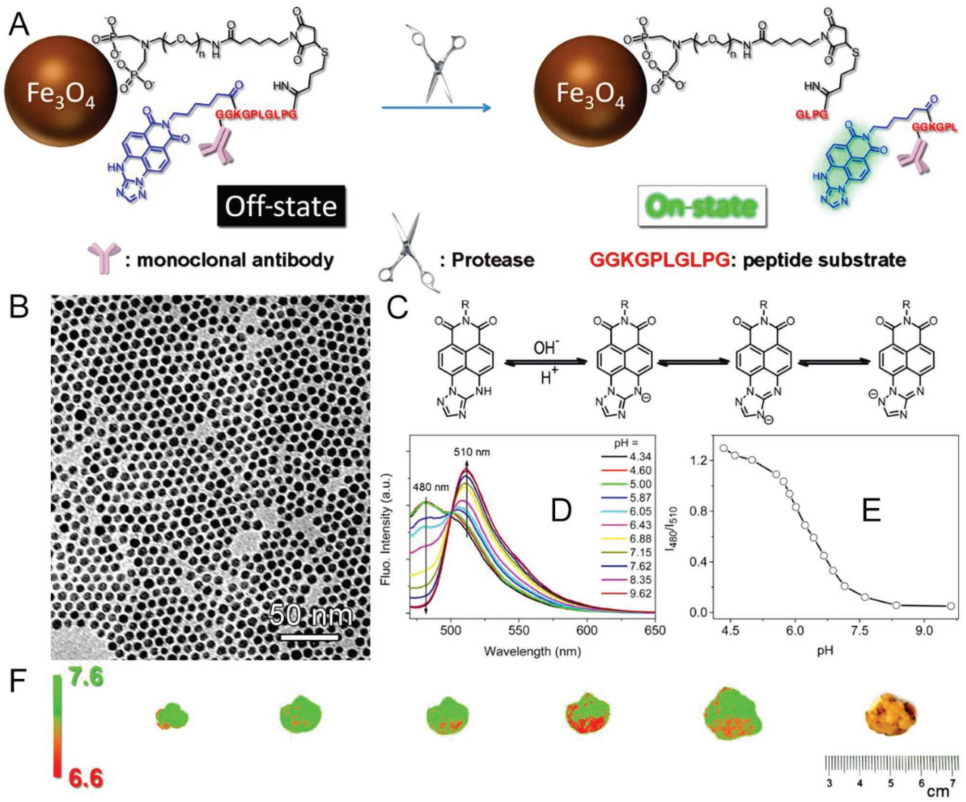

Figure 5. A) Schematic illustration of the fluorescent nanoprobe and the response to MMP-9. B) TEM image of nanoparticles. C) The pH-sensitive mechanism of ANNA. D) Fluorescence spectra of ANNA in different pH conditions. E) The pH-sensitive ratio of ANNA fluorescence. F) The pH mapping and optical image of the tumor region. Reproduced with permission.[45] Copyright 2015, American Chemical Society.

saline (PBS) buffer (20×) at different pH. The results suggest that the abnormal activity of MMP-9 is well correlated in time with abnormal lower pH in vivo. By continually imaging the tumor microenvironment for 4 days, the protease activity mapping and pH mapping results reveal that these two regions can predict the tumor invasion directions. The concept of dual-ratiometric fluorescent probe design, which achieved simultaneous quantitative monitoring of multiple microenvironment biomarkers may provide a powerful noninvasive tool for better understanding tumor progression in vivo.

Single stimuli–responsive probes provide selective and sensitive stratagem for visualization of tumor microenvironment with high signal to noise ratio. Comparing with the single stimuli–responsive probes, multistimuli ones not only provide a more exact specific imaging of tumor, avoiding the possibility of "false positive" result. In addition, individual imaging of multiparameter enables researchers to deeply understand relationship among these factors and the development of tumor.

3. Activatable MRI Nanoprobes

Similar to optical imaging nanoprobes, activatable MRI nanoprobes were also designed.[105] There are several concepts to design activatable MRI nanoprobes: tumor-associated physiological parameter–triggered release of paramagnetic ions, precisely controlling the contact between particles and surrounding protons and aggregation of magnetic NPs. In this part, these MRI nanoprobes are concluded.

3.1. Paramagnetic Ion–Released MRI Nanoprobes

Release of paramagnetic ions within cancer area is the most popular method to boost the T_1-MRI effect of nanoscale contrast agents.[106–109] Among these cations, Gd^{3+}, Mn^{2+}, and Fe^{3+} are widely used as T_1-MRI contrast agents because of their long electron spin relaxation times and high magnetic moments. Thus, various Mn- or Fe-containing nanostructures have been designed as promising MR nanoprobes for tumor microenvironment imaging by releasing Mn^{2+} or Fe^{3+}.[110–114] Such probe can response in specific area inside the tumor, thereby providing some clues for detecting and treating tumors.

Kataoka and co-workers reported an excellent pH-sensitive MRI nanoprobe based on Mn^{2+}-doped calcium phosphate (CaP) nanoparticles with poly(ethylene glycol) (PEG) coating.[115] After accumulation in tumor area through EPR effect, the CaP matrix will dissolve and release Mn^{2+} ions in the acidic tumor microenvironment, selectively enhancing T_1-MR signals in tumor region due to the Mn^{2+} interaction with the surrounding biomolecules. With pH response, such Mn^{2+}-doped CaP nanoparticles could progressively identify hypoxic tumor microenvironment for evaluating the tumor malignancy and

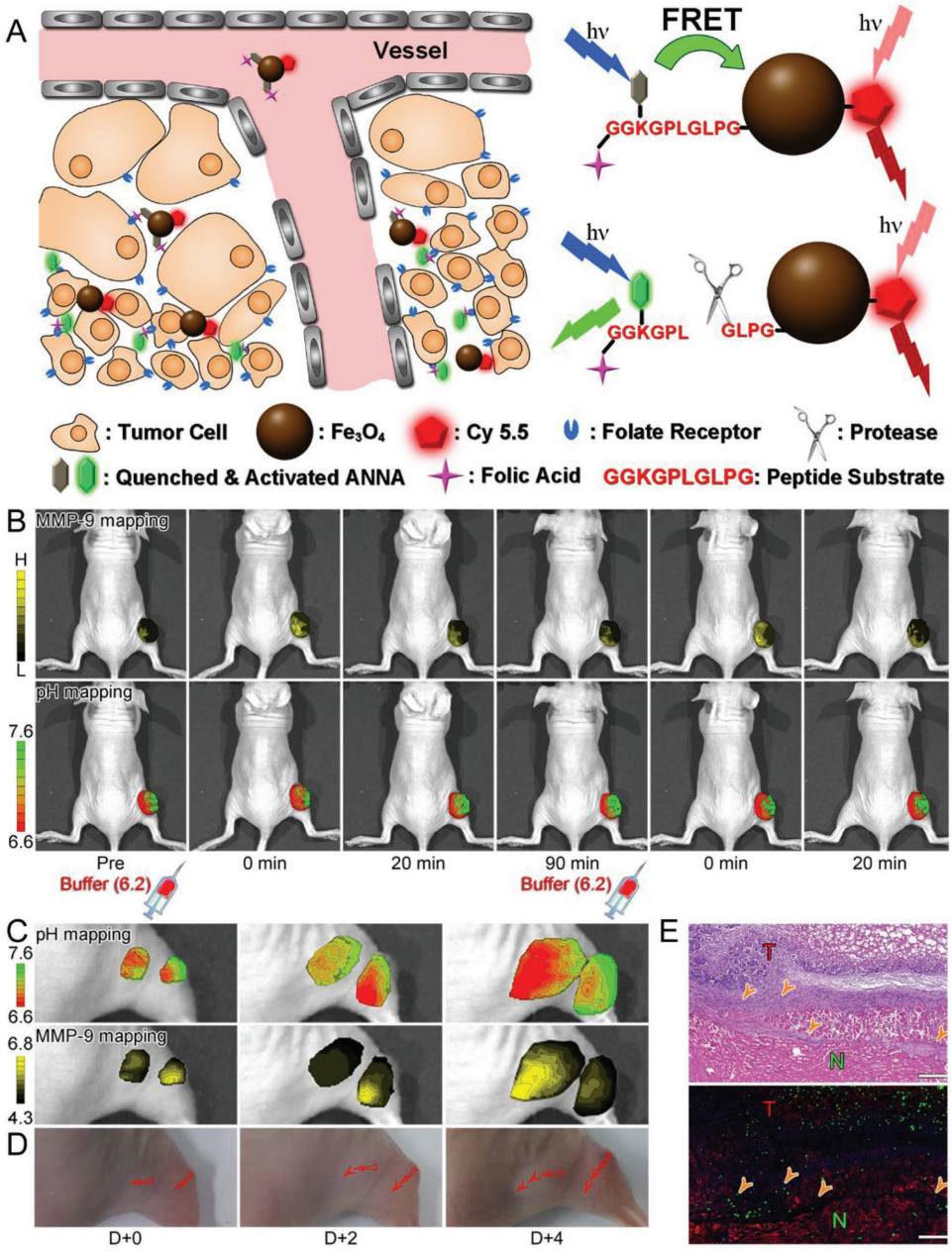

Figure 6. A) Schematic of the behavior of nanoprobes in vivo and their response to enzyme. B) The MMP-9 activity mapping after adjusting pH in tumor. C) The continuous quantified mapping of pH and MMP-9 activity in vivo. D) The continuous photographs of tumors. E) The hematoxylin and eosin (H&E) staining histology tissue image (top) and immunofluorescence image for E-cadherin expression and MMP-9 expression (bottom).The scale bars correspond to 200 µm. Reproduced with permission.[42] Copyright 2018, American Chemical Society.

further detecting small metastatic tumors via the significantly increased MR signal (**Figure 7**). This rapid and noninvasive hypoxia detection is of great significance for monitoring tumor prognosis and metastasis, which may be applied to identify the grading and staging of cancer in clinical diagnosis for some time to come.

More recently, Huang et al. prepared manganese–iron layered double hydroxide based on a coprecipitation strategy in which $Mn(NO_3)_2$ and $Fe(NO_3)_3$ serve as precursors. Such platelet-like nanostructures showed great sensitivity to the acidic tumor microenvironments and triggered the release of Mn^{2+} and Fe^{3+} ions, leading to the dramatic enhancement of T_1-MRI contrast within solid tumors.[112] Analogously, Shi and co-workers group designed a T_1-MRI contrast agent based on Mn^{2+} ions with the inner location of MnO_x in hollow mesoporous silica nanoparticles for efficiently imaging the acidic tumor microenvironment. MnO_x will dissolve under weak acidic environment and release the Mn^{2+} ions. In this case, the relaxation rate r_1 of probe can reach 8.81 mM^{-1} s^{-1} which achieves a great increase (11-fold) comparing with the neutral condition, and almost twofold higher than commercial Gd^{3+}-based contrast agents.[116] These kind of pH-responsive MRI probes can sensitively respond to

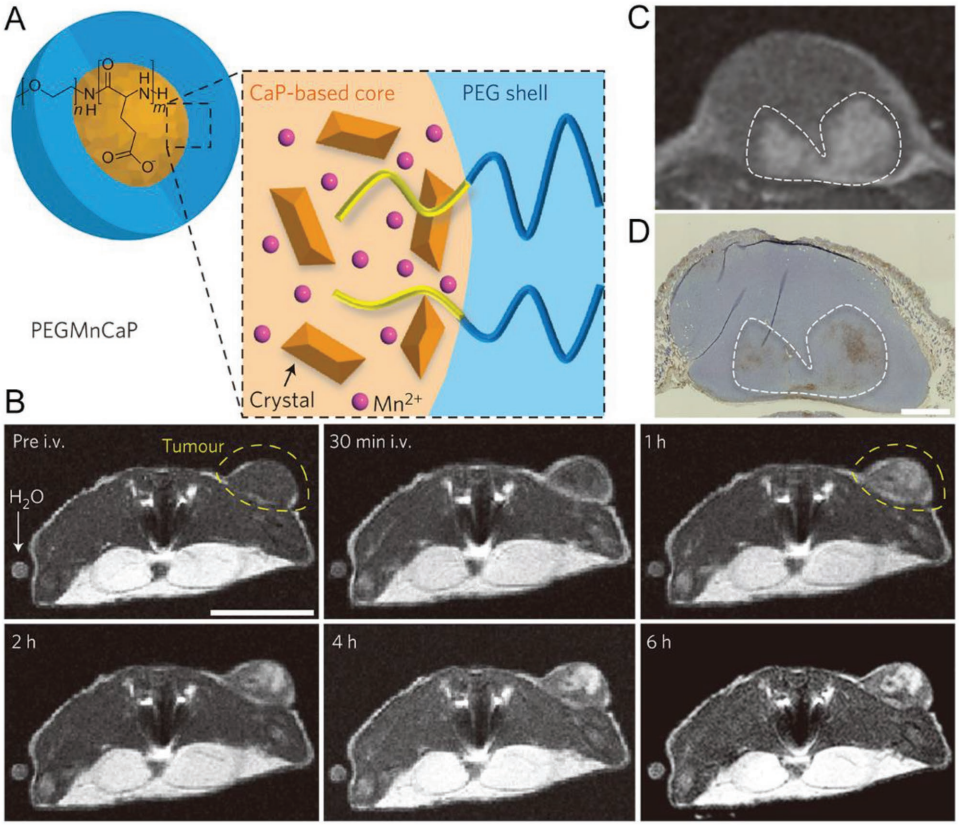

Figure 7. A) Schematic of the structure of pH-activatable nanoprobes. B) The MR images of subcutaneous C26 tumor–bearing mice before and after injection of nanoparticles. C) The MR image of the hypoxic region in tumor after injection of nanoparticles. D) The immunohistochemical image of tumor tissues with pimonidazole. Reproduced with permission.[115] Copyright 2016, Springer Nature.

the acidic microenvironment and enhance the signal apparently in the tumor site.

MnO_2 has also been developed for smart probes due to its enhanced T_1-MRI signal via releasing Mn(II) ion in the acidic tumor microenvironment. Ma et al. developed an acidic H_2O_2-responsive nanoplatform SiO_2–MB@MnO_2 with a SiO_2 core containing methylene blue (MB) as the photosensitizer of photodynamic therapy (PDT), and a MnO_2 shell to shield the core. To selectively respond to overexpressed H_2O_2 in the acidic pathological microenvironment, the MnO_2 shell can be reduced by H_2O_2, which not only generates O_2 to overcome the hypoxia, but also releases Mn(II) ion that highly improved the T_1-MRI performance for tumor imaging and detection.[117] Thus, the probe can be expected to colocalize the H_2O_2 overexpressive and acidic region, as well as treating the cancer. Liu et al. designed the multistimuli-responsive nanoplatform for cancer imaging and cancer theranostic.[118] The bovine serum albumin-stabled MnO_2 nanoparticles were modified with the cisplatin prodrug and hafnium (Hf) ions. The prodrug can be cleaved in the presence of GSH via redox process, thus the cisplatin can be released for chemotherapy. Meanwhile, the MnO_2 can generate O_2 in the presence of H_2O_2 and degraded into Mn(II) ion in the acidic condition. Hf ions can serve as radiosensitizer. As a result, this probe can respond to multistimuli including redox, low pH, and H_2O_2 in tumor microenvironment for imaging and therapy.

3.2. Surface Screening MRI Nanoprobes

Nanoenvironmental interface refers to the interface between nanoparticle and the molecules in the surrounding environment. The fundamental principle of nanoparticle as a contrast agent is based on changing the transverse relaxation time of its surrounding water protons, therefore it is possible to construct microenvironment-sensitive MRI contrast agent by adjusting the interaction between nanoparticles and surrounding water molecules.[57,119] Based on this, coating a shell on the surface of nanoparticle which can shield the contact between nanoparticles and water molecules under normal conditions but dissolve to expose the NP surface in the microenvironment and consequently obtain increased enhancement of MR signal in the tumor site is a feasible idea to design surface screening–responsive MRI nanoprobe.

A number of pH-sensitive MRI nanoprobes through encapsulating Fe_3O_4 nanoparticle with acid degraded polymeric micelles were developed to act as intelligent contrast agent, which was responded fleetly to an acidic microenvironment for MRI.[120,121] The polymeric micelle consisting of PEG and a pH-sensitive poly(β-amino ester) could be self-assembled at physiological pH, which made Fe_3O_4 NPs show limited T_2 contrast ability because of the isolation state between water molecules and these NPs. However, in the tumor site, the pH-responsive constituent ionizable *tert*-amino groups can become protonated

to be soluble and expose the Fe_3O_4 NPs to water molecules, subsequently resulting in remarkably enhanced T_2-MRI contrast.

Lately, Fan et al. prepared an acidity-sensitive fluorescence/MR dual-model probes (S-NP) via encapsulating the photosensitizer chlorin e6 (Ce6) and Gd complex for imaging-guided treatment. The S-NP has a distinct three-layer nanostructure, and the middle layer can be dismantled by the slightly acidic microenvironment due to the amide bond cleavage. As a result, the PEG shell of S-NP will be deshielded, and water molecules around the NPs obtain more access to the open coordination site of Gd complex and enlarged MR signal intensity.[122]

In general, removing the surface polymer layer within tumor microenvironment to induce more frequent interaction between the nanoparticles and the ambient water protons is a practical way to design responsive MRI nanoprobe. But perhaps more usefully, some antitumor drugs can be embedded in the polymer layer, and will be released during the decomposition. Therefore, the MR imaging can not only selectively reveal the change of tumor microenvironment, but also monitor drug release.

3.3. Aggregation-Induced Enhancement MRI Nanoprobes

Aggregation of nanoagents is also a feasible strategy to enhance MRI signal intensity or to achieve conversion between T_1 and T_2 contrast in specific areas within tumor. The MRI relativities of iron oxide nanoparticles (IONPs) are closely related to their diameter. IONPs with a tiny size (<5 nm) and highly dispersed state can generate high T_1-weighted MRI signal. The Fe ions on these nanoparticle surfaces can significantly affect both the longitudinal and transverse relaxation times of surrounding water protons.[61,105] However, after tiny-sized IONPs assemble together, T_2 relaxation will gradually accelerate, leading to a strong enhancement of T_2 contrast signal. Thus, IONPs can serve as an effective switch/transition MRI contrast agent. Motivated by this interesting property, Wang et al. prepared the 3.5 nm ultrafine iron oxide nanoparticle (uIONP) with preferable cancerous tissue permeability. Such uIONPs can assemble together and develop into clusters in the acid tumor microenvironment, which not only prevent the nanoparticles from backing into the blood or lymphatic vessels, but also accomplish T_1 to T_2 contrast switching.[123]

In addition, aggregation of NPs can also lead to the enhancement of T_1 contrast effect. Li and co-workers developed a kind of gold nanoparticles carrying Gd chelation on the surface.[124] The acidic tumor environment triggers the assembly of NPs with the concomitant activation of magnetic resonance signal improvement. Specifically, the r_1 value of nanoprobe could reach 5.6 m M^{-1} s^{-1} at pH 6.5, significantly higher than 5.1 m M^{-1} s^{-1} under pH 7.4 after 8 h incubation.

Besides acidic pH, enzyme digestion is another kind of methodology that can be used as the activated switch of aggregation. Within the tumor microenvironment, several proteases or proteolytic enzymes are highly expressed in extracellular matrix. Thus, modifying enzymes' corresponding substrates on the surface of the nanoparticles, thereby controlling their behavior within tumor region via cleavage of substrates, could be a possible way to construct microenvironment-responsive probes. Accordingly, Gallo et al. synthesized two sets of IONPs which had modified the substrates of MMP enzymes. After the cleavage of these substrates in the microenvironment, the azide or alkyne groups on either set of NPs would be exposed and selectively underwent a bio-orthogonal reaction with each other, thereby resulting in a self-assembled super-paramagnetic nanocluster network with T_2 signal enhancement properties.[125]

Analogously, Chen and co-workers prepared hyaluronic acid (HA)-coated iron oxide nanoparticles (Fe_3O_4@HA) with a small-sized magnetic core and good penetration ability to obtain clear T_1-weighted MRI images of the tumor. Responding to the HAase in the acidic tumor environment, the surface HA of probe would be degraded, and the primary iron oxide cores would aggregate to weaken T_1 and increase T_2 signal, thereby achieving the T_1 to T_2 signal shifting in the inner tumor. Thus, T_1- and T_2-weighted MRI images could be obtained at different time points and different positions in solid tumor to help with the related diagnostics.[126]

Protein- or enzyme-triggered MRI nanoprobes have also been developed. Liang and co-workers reported an enzyme-sensitive condensation to self-assemble Fe_3O_4@1 NPs in apoptotic cells of tumor for greatly enhanced T_2 MRI (**Figure 8**).[43] Caspase-3/7, one of the important biomarkers of early apoptosis, instructed the aggregation of Fe_3O_4@1 NPs (r_2 = 185 mM^{-1} s^{-1}), which induced an ≈65% increase of r_2 value when compared to the control group (r_2 = 112 mM^{-1} s^{-1}). More importantly, both in vitro and in vivo MRI experiments revealed that Fe_3O_4@1 NPs provided specific T_2-enhanced contrast in apoptotic situation, whereas the control Fe_3O_4@1-Scr NPs displayed no MR signal enhancement. After Fe_3O_4@1 NPs injected, the T_2-weighted coronal MRI of doxorubicin (DOX)-treated mice shows that the probes provide a feasible MRI strategy for evaluating therapeutic efficiency and helpful for evaluating the curative effect of proapoptotic antitumor drug in near future.

Compared with the narrow range of pH change in tumor area, the expression of enzyme in different intratumoral regions is quite different. Therefore, the enzyme-induced aggregation probe has better specificity, which is able to show the internal state of tumor more accurately.

Redox species including GSH, H_2O_2, O_2•, •OH, and so on, can also serve as triggers to the aggregations of the responsive probes. Li et al. designed an activatable nanoprobe for tumor cell recognition through connecting T_2 contrast agent (Fe_3O_4 NPs) with T_1 contrast agent (Gd_2O_3 NPs) by cystamine which contains a disulfide linkage. The formation of nanocomplex will result in quenching T_1 signal owing to the short distance between Gd_2O_3 NPs and Fe_3O_4 NPs. T_1 signal of this nanocomplex will recover due to the cleavage of disulfide bond in GSH-rich tumor microenvironment.[127] In this strategy, the T_1-MRI signal can achieve on/off transition by adjusting the distance between a paramagnetic enhancer and a super-paramagnetic quencher, which can be called distance-dependent magnetic resonance tuning (MRET), which will be a prospective way to design microenvironment-responsive MRI nanoprobe.[128]

Recently, Gao et al. reported a type of tumor microenvironment–responsive nanoprobe which could enhance tumor MR imaging through in situ cross-linking of the Fe_3O_4 nanoparticles.[66] After the NPs' surface disulfide bond cleaving by GSH within tumor microenvironment, the exposed thiol groups

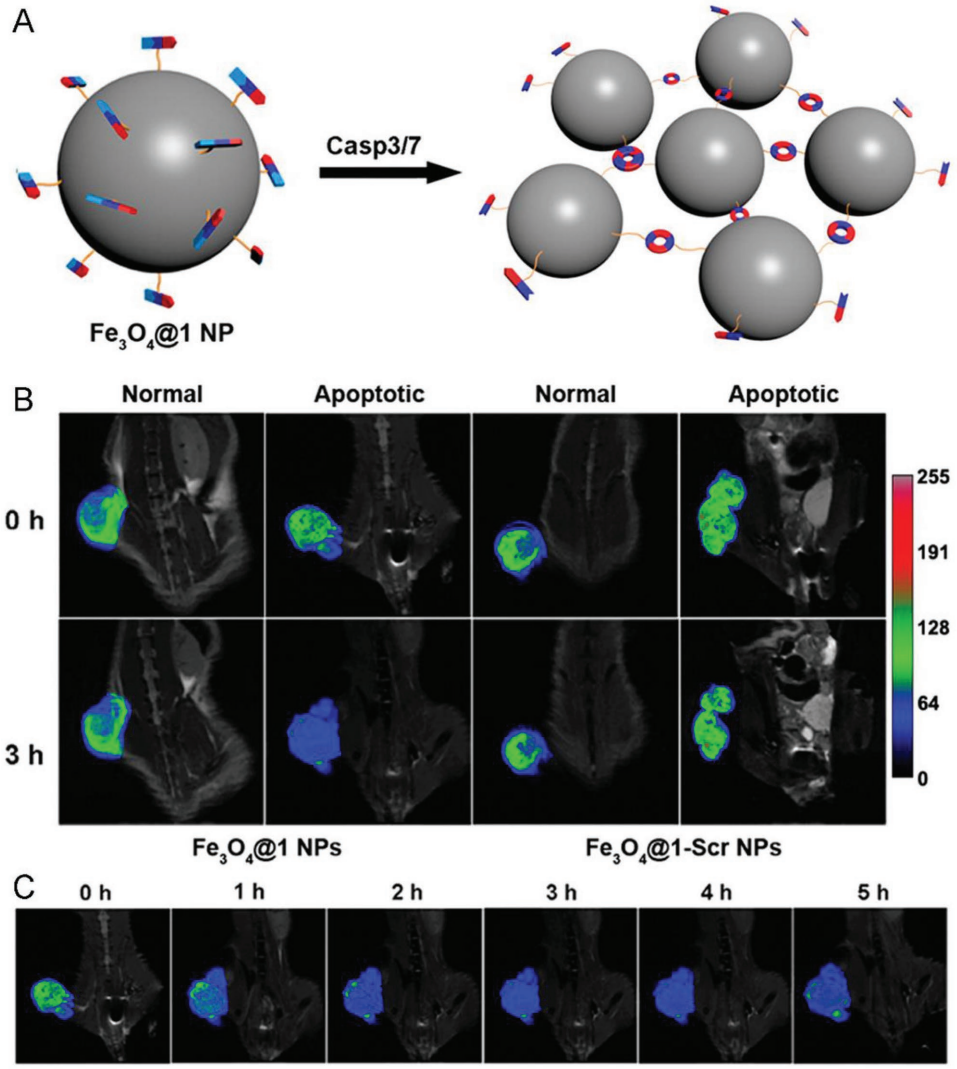

Figure 8. A) Illustration of the caspase 3/7-sensitive MRI nanoprobes. B) The in vivo MR images of saline or DOX-treated mice at 0 h (top) or 3 h (bottom) after injection of nanoprobes. C) The dynamic MR images of DOX-treated mice after injection of nanoprobes. Reproduced with permission.[43] Copyright 2016, American Chemical Society.

could react with the remaining maleimide moieties, which led to the aggregation of particles, and substantially improved the MRI contrast enhancement performance, as shown in **Figure 9**. The result of MRI in nude mice showed that with the aggregation ability of probe, T_2 value of the tumorous site reached ≈50% after 8 h intravenous injection, while the control probe only gives rise to a decrement of around 18%. Remarkably, the T_2 value recovered slowly with ΔT_2 remaining around 20% 96 h postinjection due to the self-peptide on the surface of probe, which had great potential to accomplish the in vivo long-term temporal evolution MR imaging to monitor the microenvironment of tumor area in a particular period of treatment.

4. Activatable PA Imaging Nanoprobes

PA imaging is an imaging technique upon the photoacoustic effect, which combines optical and ultrasound imaging technologies. The photoacoustic effect was first reported in 1880, but PA imaging had not been developed until the intense light sources and sensitive sensors spring up. In 1938, Veingerov reported an application of photoacoustic effect, detecting low CO_2 concentration in N_2 gas, opening the further utilization of PA imaging. In the past two decades, benefiting from the great development in the laser field and biomedical field, PA imaging has been developed to medical visualized diagnosis at anatomical or even molecular levels.[69,70,129] For ultrasensitive PA imaging in vivo, various probes based on organic chromophores or inorganic nanoparticles have been used to prepared PA contrast agents due to their excellent NIR absorbance. Recently, several pH-, enzyme-, and redox-activatable PA imaging nanoprobes have also been reported.

The stratagem for the construction of pH-sensitive PA imaging nanoprobes is based on the PA signal ratio between a pair of dyes, which have pH-dependent and pH-independent optical absorption, respectively. Chen et al. reported

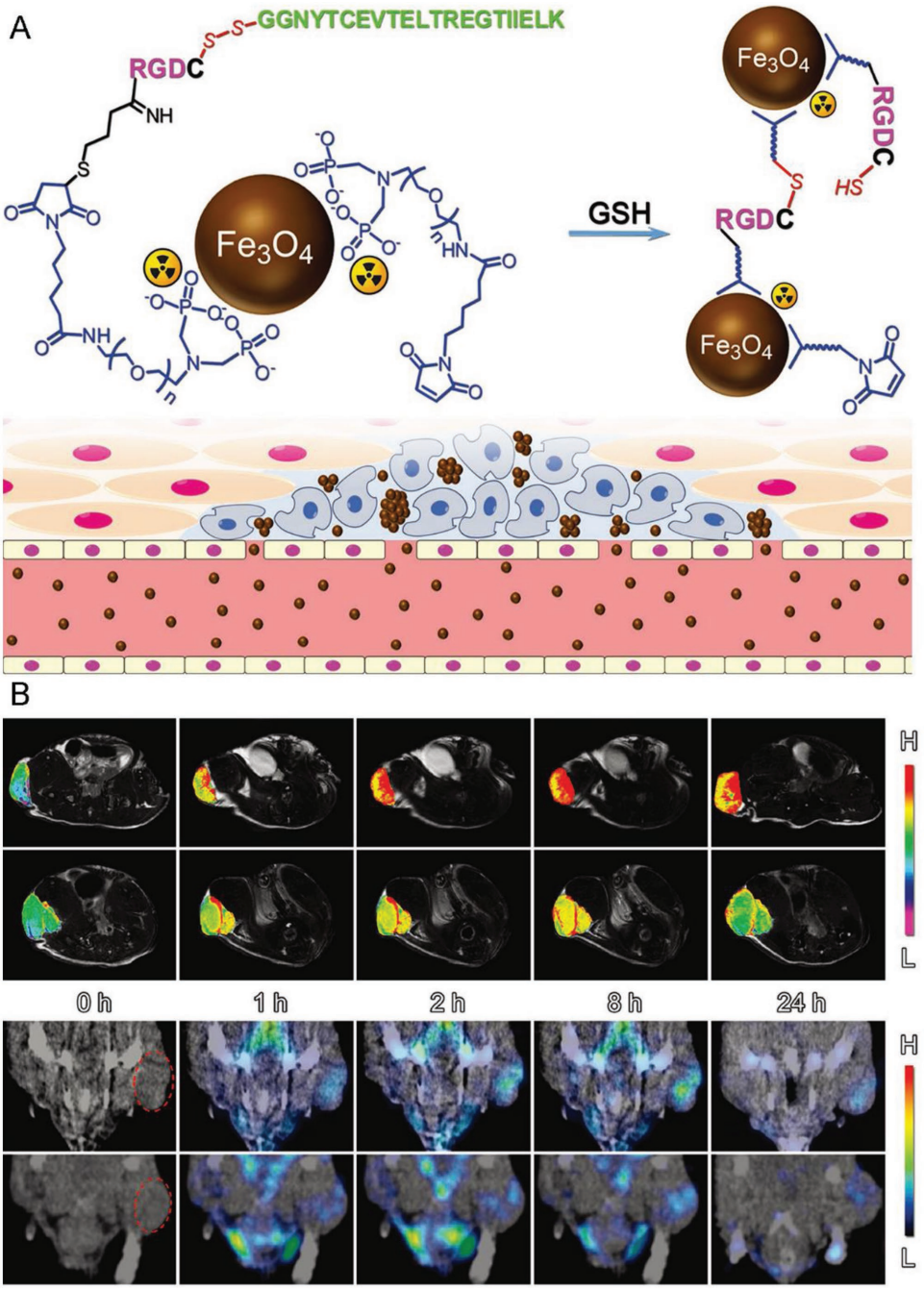

Figure 9. A) Schematic of ^{99m}Tc-labeled Fe_3O_4 NPs and their aggregation triggered by GSH within the tumor microenvironment. B) The MR image and single-photo emission computed tomography (SPECT)/computed tomography (CT) images of tumor-bearing mice after injection of the activatable nanoprobe and the control probe. Reproduced with permission.[66] Copyright 2017, Wiley-VCH.

a ratiometric photoacoustic pH-sensitive NIR nanoprobe for in vivo imaging, as shown in **Figure 10**.[72] Benzo[α]phenoxazine (BPOx) and IR825 serve as the pair of dyes. These two dyes can induce self-assembly of human serum albumin (HSA) and embedded into HSA nanoparticles. In this pair, the optical properties of IR825 is pH-independent, while BPOx performs a pH-dependent transformation under both ratiometric photoacoustic and fluorescence imaging. Therefore, two dyes' PA signal ratio and fluorescence signal ratio are both possible for measuring pH values in the acidic tumor microenvironment. After they evaluated pH detection using nanoprobe by two imaging modalities for samples under different tissue depth, the researchers found that the ratiometric values of photoacoustic signals remain almost constant along the increase of the tissue depth, and the signals were still detectable even under 10 mm tissue. On the contrary, the fluorescence signals from probe at both the wavelengths attenuated rapidly under just a thin layer of tissue (1.5 mm). In this study, comparing

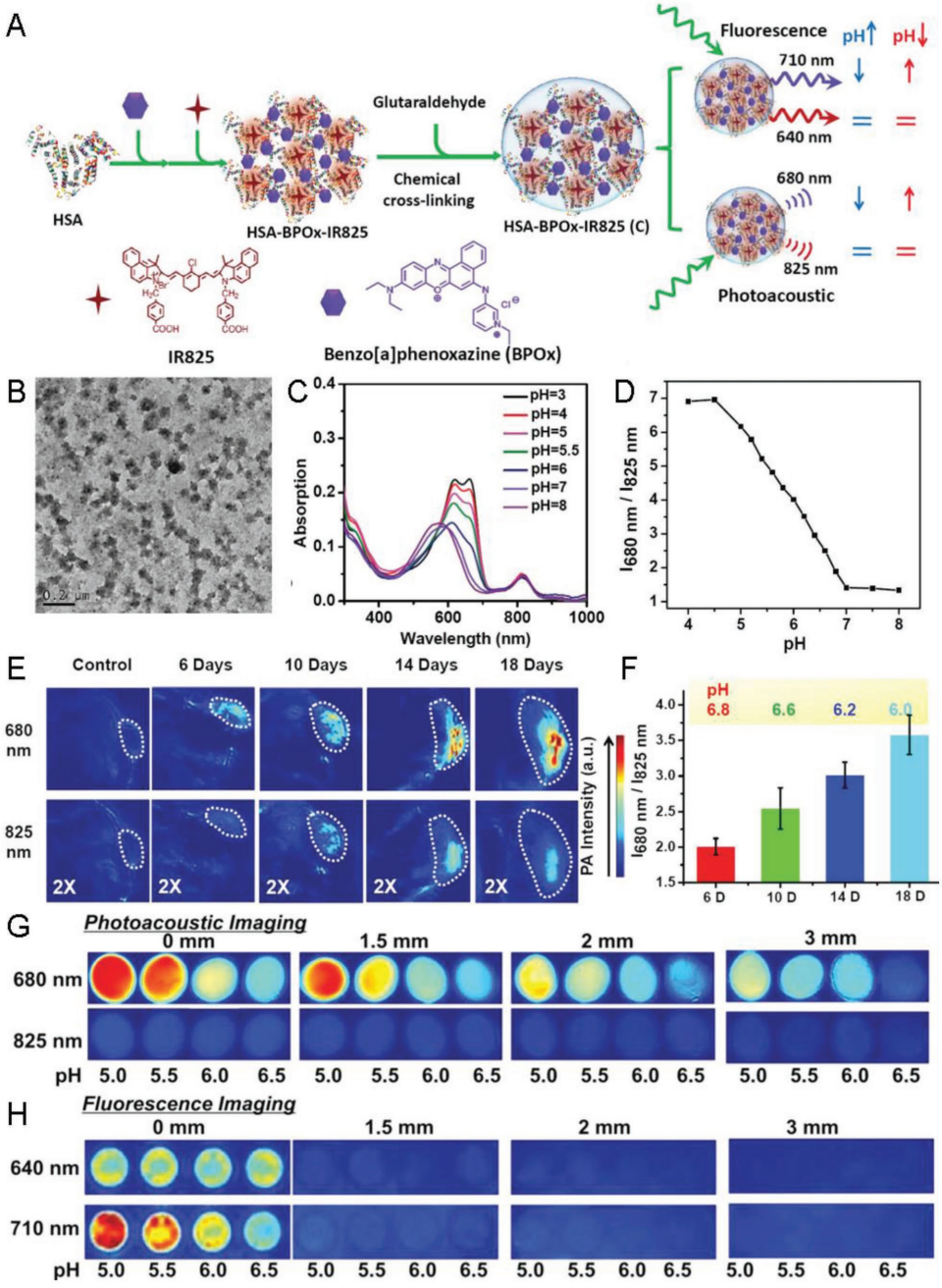

Figure 10. A) Schematic of the structure and the pH-responsive fluorescent/PA dual-modal nanoprobes. B) TEM image of nanoprobes stained by phosphotungstic acid. C) pH-dependent absorbance spectra of nanoprobes. D) The pH-dependent signal ratios of nanoprobes. E) Time-dependent PA imaging of tumor-bearing mice after injection of nanoprobes. F) I_{680}/I_{825} signal intensity ratios of tumors according to data in (E). G) The PA imaging of nanoprobes in different pH conditions, with pork tissue covered. H) The fluorescent imaging of nanoprobes in different pH conditions, with pork tissue covered. Reproduced with permission.[72] Copyright 2015, Wiley-VCH.

with traditional fluorescence imaging modality, PA imaging provided in vivo tumor microenvironmental pH imaging with improved spatial resolution and enhanced penetration depth. And, anatomical images of the mice proved the potential application for 3D image of tumor microenvironment.

PeT can also be used to build the pH-sensitive PA probes. Miao et al. reported a pH-activatable ratiometric PA imaging probe based on semiconducting oligomer (SO) nanoparticles.[130] The nanoprobe is synthesized by nanoprecipitation method using the amphiphilic triblock copolymer, SO, and the boron-dipyrromethene (pH-BDP). PeT occurs between pH-BDP and SO, leading to the silent fluorescence of SO and the enhanced PA signals of nanoparticles. The SO has a pH-independent absorption peak at 680 nm, while pH-BDP has a pH-sensitive absorption peak at 750 nm. In vivo imaging demonstrated that the PA signal can be detected clearly at the

depth of 2 cm which shows enhanced penetration depth. The pH value in tumor microenvironment was indicated in vivo by the ratiometric PA signal (PA_{680}/PA_{750}) after injection of probes into the tumor-bearing mice.

The reversible aggregation of materials is not only used to establish pH-sensitive nanoparticles, but also developed nanoprobes that are subjected to rapid metabolism in normal tissues under neutral condition, and pretend to be retained in acidic tumor microenvironment. Zeng et al. reported a novel pH-sensitive photoacoustic imaging agent based on Fe(III)–gallic acid nanoparticles.[71] The activatable PA imaging nanoprobes keep stable under acidic condition (pH 5.0), but gradually dissolve in neutral environment (pH 7.0). In vivo experiments demonstrated that the PA signal in normal organs including liver and spleen decreased to the background level after injection 24 h. This revealed the quick metabolization of the probes in these organs. On the contrary, the PA signal of nanoprobes in tumor microenvironment was still clearly detectable after 24 h postinjection because of the high stability of these probes in acidic tumor microenvironment.

Although many pH-sensitive PA imaging probes are developed, the background absorption interference in different tissues must be taken into consideration to accurately measure microenvironmental pH in vivo. Considering the oxygenated hemoglobin (HbO_2) and deoxygenated hemoglobin (Hb), Jo et al. developed an activatable PA imaging contrast agent for quantitative pH mapping in vivo.[131] The pH-sensitive nanoprobes were prepared by encapsulating an optical pH indicator (5-(and-6)-carboxylic acid) into polyacrylamide nanoparticles (PAA NPs). The absorption of the indicator at 565 nm presents a pH-independent point, while the 600 nm point closely associated with the different pH. Furthermore, 576 and 584 nm points were also measured to correct the background tissue affect considering the optical absorption of HbO_2 and Hb. Accurate quantitative pH mapping in vivo can be achieved by quad-wavelength PA signal measurement and the error was less than 0.16 pH at 6 mm depth in tissue.

For enzyme-sensitive PA imaging, the cleavage of peptide by certain enzyme is a typical method which has been already utilized in other traditional detection techniques including fluorescence imaging and MR imaging. To build enzyme-sensitive PA imaging contrast agent, two chromophores, BHQ3 and Aleca750 were linked by Geeee[Ahx]PLGLAGrrrrrK, which can be cleaved by MMP-2.[73] In the intact state, these two chromophores showed two PA signals at 675 and 750 nm with similar intensity. In MMP-2-rich microenvironment, the cleavage of the peptide linker caused that only the PA signal of BHQ3, which accumulates in the tumor cells, can be seen. On the contrary, the other dye would diffuse away. Therefore, subtraction of the PA signal intensity at two wavelengths indicates the high activity of MMP-2. Based on similar enzyme-sensitive cleavage mechanism, Ai et al. described a strategy for tumor localization by enzyme-induced cross-linking of UCNPs.[132] The Nd^{3+}-doped UCNPs were modified with PAA and polyethylenimine (PEI), which further connected with Ce6 and an enzyme-sensitive peptide. After cathepsin B (Cts B), whose upregulation is generally observed in tumor microenvironment, cleaves the peptide, the exposed cysteine and 2-cyanobenzothiazole will react with each other, inducing the covalent cross-linking among UCNPs. Such enzyme-sensitive cross-linking of UCNPs results in the increase of upconversion luminescence, the decrease of PA signal, and the enhanced reactive singlet oxygen generation.

5. Conclusion and Outlook

In this review, recent achievements of activatable molecular imaging nanoprobes for tumor-associated microenvironment detection including optical imaging, MR imaging, and PA imaging were summarized. Comparing with small molecular activatable imaging probes, nanoprobes are considered as a promising platform to design responsive mechanism upon different stimuli including O_2, acidic condition, specific enzyme, redox, and so on, because their large specific surface area offers a big room to modified functional moieties. Although fruitful achievements have been reported in this area, great challenges remain in the development of activatable nanoprobes for tumor microenvironment imaging in vivo. For instance, because the progression of tumor is closely associated with multiphysiological factors in microenvironment, designing multisensitive mechanisms is meaningful for fundamental studies and clinical applications. Furthermore, researchers still need to make great efforts to discover relevant biomarkers for understanding the tumor mechanism, and find their activatable strategies. Finally, a few researches have demonstrated the potential application of responsive imaging nanoprobes in clinic, including the image-guided surgery, drug control release, evaluating therapeutic efficacy, and photothermal therapy. However, strenuous efforts still need to revolve around developing strategies to upload anticancer agents with the nanoprobes for constructing stimuli-responsive smart diagnostic and theranostic nanoplatforms.

Acknowledgements

T.C.M. and P.S.Z. contributed equally to this work. The authors thank the National Natural Science Foundation of China (NSFC) (Grant Nos. 81471726, 81671754, 81530057, 81671755, 81771902, 81720108024) and the CAS (Grant Nos. 2016YZ01, PY-2015-32) for financial support.

Conflict of Interest

The authors declare no conflict of interest.

Keywords

activatable molecular imaging nanoprobe, magnetic resonance imaging, optical imaging, photoacoustic imaging, tumor microenvironments

Received: April 14, 2018
Revised: June 14, 2018
Published online:

[1] J. M. Brown, W. R. William, *Nat. Rev. Cancer* **2004**, *4*, 437.
[2] B. A. Webb, M. Chimenti, M. P. Jacobson, D. L. Barber, *Nat. Rev. Cancer* **2011**, *11*, 671.

[3] V. Estrella, T. A. Chen, M. Lloyd, J. Wojtkowiak, H. H. Cornnell, A. Ibrahim-Hashim, K. Bailey, Y. Balagurunathan, J. M. Rothberg, B. F. Sloane, J. Johnson, R. A. Gatenby, R. J. Gillies, *Cancer Res.* **2013**, *73*, 1524.
[4] J. Rozhin, M. Sameni, G. Ziegler, B. F. Sloane, *Cancer Res.* **1994**, *54*, 6517.
[5] D. Hanahan, R. A. Weinberg, *Cell* **2011**, *144*, 646.
[6] K. Kessenbrock, V. Plaks, Z. Werb, *Cell* **2010**, *141*, 52.
[7] M. A. Moses, D. Wiederschain, K. R. Loughlin, D. Zurakowski, C. C. Lamb, M. R. Freeman, *Cancer Res.* **1998**, *58*, 1395.
[8] M. J. Farquharson, A. Al-Ebraheem, G. Falkenberg, R. Leek, A. L. Harris, D. A. Bradley, *Phys. Med. Biol.* **2008**, *53*, 3023.
[9] G. L. Semenza, *BBA, Biochim. Biophys. Acta, Mol. Cell Res.* **2016**, *1863*, 382.
[10] T. R. Cox, R. M. H. Rumney, E. M. Schoof, L. Perryman, A. M. Hoye, A. Agrawal, D. Bird, N. Ab Latif, H. Forrest, H. R. Evans, I. D. Huggins, G. Lang, R. Linding, A. Gartland, J. T. Erler, *Nature* **2015**, *522*, 106.
[11] A. L. Harris, *Nat. Rev. Cancer* **2002**, *2*, 38.
[12] O. Warburg, K. Posener, E. Negelein, *Biochem. Z.* **1924**, *152*, 309.
[13] R. A. Gatenby, E. T. Gawlinski, A. F. Gmitro, B. Kaylor, R. J. Gillies, *Cancer Res.* **2006**, *66*, 5216.
[14] Q. Shi, X. D. Le, B. L. Wang, J. L. Abbruzzese, Q. H. Xiong, Y. J. He, K. P. Xie, *Oncogene* **2001**, *20*, 3751.
[15] F. Mbeunkui, D. J. Johann, *Cancer Chemother. Pharmacol.* **2009**, *63*, 571.
[16] M. Allinen, R. Beroukhim, L. Cai, C. Brennan, J. Lahti-Domenici, H. Y. Huang, D. Porter, M. Hu, L. Chin, A. Richardson, S. Schnitt, W. R. Sellers, K. Polyak, *Cancer Cell* **2004**, *6*, 17.
[17] M. Nordsmark, S. M. Bentzen, V. Rudat, D. Brizel, E. Lartigau, P. Stadler, A. Becker, M. Adam, M. Molls, J. Dunst, D. J. Terriis, J. Overgaard, *Radiother. Oncol.* **2005**, *77*, 18.
[18] A. W. Fyles, M. Milosevic, R. Wong, M. C. Kavanagh, M. Pintilie, A. Sun, W. Chapman, W. Levin, L. Manchul, T. J. Keane, R. P. Hill, *Radiother. Oncol.* **1998**, *48*, 149.
[19] A. Fyles, M. Milosevic, D. Hedley, M. Pintilie, W. Levin, L. Manchul, R. P. Hill, *J. Clin. Oncol.* **2002**, *20*, 680.
[20] M. Milosevic, P. Warde, C. Menard, P. Chung, A. Toi, A. Ishkanian, M. Mclean, M. Pintilie, J. Sykes, M. Gospodarowicz, C. Catton, R. P. Hill, R. Bristow, *Clin. Cancer Res.* **2012**, *18*, 2108.
[21] J. B. Antonsson, C. C. Boyle, K. L. Kruithoff, H. L. Wang, E. Sacristan, H. R. Rothschild, M. P. Fink, *Am. J. Physiol.* **1990**, *259*, G519.
[22] A. Kurkdjian, J. Guern, *Annu. Rev. Plant Physiol. Plant Mol. Biol.* **1989**, *40*, 271.
[23] H. R. Herschman, *Science* **2003**, *302*, 605.
[24] P. P. Provenzano, K. W. Eliceiri, P. J. Keely, *Trends Cell Biol.* **2009**, *19*, 638.
[25] R. Weissleder, *Nat. Rev. Cancer* **2002**, *2*, 11.
[26] R. M. Hoffman, *Nat. Rev. Cancer* **2005**, *5*, 796.
[27] M. Yang, L. N. Li, P. Jiang, A. R. Moossa, S. Penman, R. M. Hoffman, *Proc. Natl. Acad. Sci. USA* **2003**, *100*, 14259.
[28] J. Condeelis, J. E. Segall, *Nat. Rev. Cancer* **2003**, *3*, 921.
[29] E. B. Brown, R. B. Campbell, Y. Tsuzuki, L. Xu, P. Carmeliet, D. Fukumura, R. K. Jain, *Nat. Med.* **2001**, *7*, 1069.
[30] W. R. Wilson, M. P. Hay, *Nat. Rev. Cancer* **2011**, *11*, 393.
[31] T. D. Ashton, K. A. Jolliffe, F. M. Pfeffer, *Chem. Soc. Rev.* **2015**, *44*, 4547.
[32] L. Leng, Y. B. Wang, N. N. He, D. Wang, Q. J. Zhao, G. W. Feng, W. J. Su, Y. Xu, Z. C. Han, D. L. Kong, Z. Cheng, R. Xiang, Z. J. Li, *Biomaterials* **2014**, *35*, 5162.
[33] R. R. Qiao, J. F. Zeng, Q. J. Jia, J. Du, L. Shen, M. Y. Gao, *Acta Phys.-Chim. Sin.* **2012**, *28*, 993.
[34] L. H. Jing, K. Ding, S. V. Kershaw, I. M. Kempson, A. L. Rogach, M. Y. Gao, *Adv. Mater.* **2014**, *26*, 6367.
[35] C. Y. Liu, Y. Hou, M. Y. Gao, *Adv. Mater.* **2014**, *26*, 6922.
[36] R. Qiao, C. Yang, M. Gao, *J. Mater. Chem.* **2009**, *19*, 9286.
[37] Z. Gao, T. Ma, E. Zhao, D. Docter, W. Yang, R. H. Stauber, M. Gao, *Small* **2016**, *12*, 556.
[38] M. Jiao, P. Zhang, J. Meng, Y. Li, C. Liu, X. Luo, M. Gao, *Biomater. Sci.* **2018**, *6*, 726.
[39] J. J. Li, F. F. Cheng, H. P. Huang, L. L. Li, J. J. Zhu, *Chem. Soc. Rev.* **2015**, *44*, 7855.
[40] Y. Matsumura, H. Maeda, *Cancer Res.* **1986**, *46*, 6387.
[41] N. Bertrand, J. Wu, X. Xu, N. Kamaly, O. C. Farokhzad, *Adv. Drug Delivery Rev.* **2014**, *66*, 2.
[42] T. Ma, Y. Hou, J. Zeng, C. Liu, P. Zhang, L. Jing, D. Shangguan, M. Gao, *J. Am. Chem. Soc.* **2018**, *140*, 211.
[43] Y. Yuan, Z. Ding, J. Qian, J. Zhang, J. Xu, X. Dong, T. Han, S. Ge, Y. Luo, Y. Wang, K. Zhong, G. Liang, *Nano Lett.* **2016**, *16*, 2686.
[44] C. C. You, O. R. Miranda, B. Gider, P. S. Ghosh, I. B. Kim, B. Erdogan, S. A. Krovi, U. H. F. Bunz, V. M. Rotello, *Nat. Nanotechnol.* **2007**, *2*, 318.
[45] Y. Hou, J. Zhou, Z. Gao, X. Sun, C. Liu, D. Shangguan, W. Yang, M. Gao, *ACS Nano* **2015**, *9*, 3199.
[46] H. F. Shi, H. B. Sun, H. R. Yang, S. J. Liu, G. Jenkins, W. Feng, F. Y. Li, Q. Zhao, B. Liu, W. Huang, *Adv. Funct. Mater.* **2013**, *23*, 3268.
[47] I. L. Medintz, H. T. Uyeda, E. R. Goldman, H. Mattoussi, *Nat. Mater.* **2005**, *4*, 435.
[48] F. Helmchen, W. Denk, *Nat. Methods* **2005**, *2*, 932.
[49] C. Liu, Y. Qi, R. Qiao, Y. Hou, K. Chan, Z. Li, J. Huang, L. Jing, J. Du, M. Gao, *Nanoscale* **2016**, *8*, 12579.
[50] R. R. Qiao, C. H. Liu, M. H. Liu, H. Hu, C. Y. Liu, Y. Hou, K. C. Wu, Y. N. Lin, J. M. Liang, M. Y. Gao, *ACS Nano* **2015**, *9*, 2120.
[51] C. Y. Liu, W. Ma, Z. Y. Gao, J. Y. Huang, Y. Hou, C. L. Xu, W. S. Yang, M. Y. Gao, *J. Mater. Chem. C* **2014**, *2*, 9637.
[52] Y. Hou, R. R. Qiao, F. Fang, X. X. Wang, C. Y. Dong, K. Liu, C. Y. Liu, Z. F. Liu, H. Lei, F. Wang, M. Y. Gao, *ACS Nano* **2013**, *7*, 330.
[53] C. Y. Liu, Z. Y. Gao, J. F. Zeng, Y. Hou, F. Fang, Y. L. Li, R. R. Qiao, L. Shen, H. Lei, W. S. Yang, M. Y. Gao, *ACS Nano* **2013**, *7*, 7227.
[54] Q. Liu, W. Feng, T. Yang, T. Yi, F. Li, *Nat. Protoc.* **2013**, *8*, 2033.
[55] Y. Dai, H. Xiao, J. Liu, Q. Yuan, P. a. Ma, D. Yang, C. Li, Z. Cheng, Z. Hou, P. Yang, J. Lin, *J. Am. Chem. Soc.* **2013**, *135*, 18920.
[56] D. K. Chatteriee, A. J. Rufalhah, Y. Zhang, *Biomaterials* **2008**, *29*, 937.
[57] D. Ling, W. Park, S.-j. Park, Y. Lu, K. S. Kim, M. J. Hackett, B. H. Kim, H. Yim, Y. S. Jeon, K. Na, T. Hyeon, *J. Am. Chem. Soc.* **2014**, *136*, 5647.
[58] J. Park, K. J. An, Y. S. Hwang, J. G. Park, H. J. Noh, J. Y. Kim, J. H. Park, N. M. Hwang, T. Hyeon, *Nat. Mater.* **2004**, *3*, 891.
[59] S. H. Sun, H. Zeng, *J. Am. Chem. Soc.* **2002**, *124*, 8204.
[60] J. W. Cheon, N. J. Kang, S. M. Lee, J. H. Lee, J. H. Yoon, S. J. Oh, *J. Am. Chem. Soc.* **2004**, *126*, 1950.
[61] B. H. Kim, N. Lee, H. Kim, K. An, Y. I. Park, Y. Choi, K. Shin, Y. Lee, S. G. Kwon, H. B. Na, J. G. Park, T. Y. Ahn, Y. W. Kim, W. K. Moon, S. H. Choi, T. Hyeon, *J. Am. Chem. Soc.* **2011**, *133*, 12624.
[62] F. Q. Hu, L. Wei, Z. Zhou, Y. L. Ran, Z. Li, M. Y. Gao, *Adv. Mater.* **2006**, *18*, 2553.
[63] S. J. Liu, B. Jia, R. R. Qiao, Z. Yang, Z. L. Yu, Z. F. Liu, K. Liu, J. Y. Shi, O. Y. Han, F. Wang, M. Y. Gao, *Mol. Pharmaceutics* **2009**, *6*, 1074.
[64] F. Q. Hu, Q. J. Jia, Y. L. Li, M. Y. Gao, *Nanotechnology* **2011**, *22*, 245604.
[65] Q. J. Jia, J. F. Zeng, R. R. Qjao, L. H. Jing, L. Peng, F. L. Gu, M. Y. Gao, *J. Am. Chem. Soc.* **2011**, *133*, 19512.
[66] Z. Gao, Y. Hou, J. Zeng, L. Chen, C. Liu, W. Yang, M. Gao, *Adv. Mater.* **2017**, *29*, 1701095.
[67] G. Liang, J. Ronald, Y. Chen, D. Ye, P. Pandit, M. L. Ma, B. Rutt, J. Rao, *Angew. Chem., Int. Ed.* **2011**, *50*, 6283.
[68] Y. Yuan, H. Sun, S. Ge, M. Wang, H. Zhao, L. Wang, L. An, J. Zhang, H. Zhang, B. Hu, J. Wang, G. Liang, *ACS Nano* **2015**, *9*, 761.
[69] C. Kim, C. Favazza, L. H. V. Wang, *Chem. Rev.* **2010**, *110*, 2756.

[70] L. V. Wang, S. Hu, *Science* **2012**, *335*, 1458.
[71] J. F. Zeng, M. Cheng, Y. Wang, L. Wen, L. Chen, Z. Li, Y. Y. Wu, M. Y. Gao, Z. F. Chai, *Adv. Healthcare. Mater.* **2016**, *5*, 772.
[72] Q. Chen, X. Liu, J. Chen, J. Zeng, Z. Cheng, Z. Liu, *Adv. Mater.* **2015**, *27*, 6820.
[73] J. Levi, S. R. Kothapalli, T. J. Ma, K. Hartman, B. T. Khuri-Yakub, S. S. Gambhir, *J. Am. Chem. Soc.* **2010**, *132*, 11264.
[74] M. C. Brahimi-Horn, J. Chiche, J. Pouyssegur, *J. Mol. Med.* **2007**, *85*, 1301.
[75] R. A. Gatenby, R. J. Gillies, *Nat. Rev. Cancer* **2004**, *4*, 891.
[76] J. Pouyssegur, F. Dayan, N. M. Mazure, *Nature* **2006**, *441*, 437.
[77] F. Perche, S. Biswas, T. Wang, L. Zhu, V. P. Torchilin, *Angew. Chem., Int. Ed.* **2014**, *53*, 3362.
[78] G. Q. Zhang, G. M. Palmer, M. Dewhirst, C. L. Fraser, *Nat. Mater.* **2009**, *8*, 747.
[79] X. C. Zheng, X. Wang, H. Mao, W. Wu, B. R. Liu, X. Q. Jiang, *Nat. Commun.* **2015**, *6*, 5834.
[80] X. C. Zheng, H. Tang, C. Xie, J. L. Zhang, W. Wu, X. Q. Jiang, *Angew. Chem., Int. Ed.* **2015**, *54*, 8094.
[81] E. J. Mclaurin, A. B. Greytak, M. G. Bawendi, D. G. Nocera, *J. Am. Chem. Soc.* **2009**, *131*, 12994.
[82] M. Amelia, A. Lavie-Cambot, N. D. Mcclenaghan, A. Credi, *Chem. Commun.* **2011**, *47*, 325.
[83] J. N. Liu, Y. Liu, W. B. Bu, J. W. Bu, Y. Sun, J. L. Du, J. L. Shi, *J. Am. Chem. Soc.* **2014**, *136*, 9701.
[84] Y. L. Chiu, S. A. Chen, J. H. Chen, K. J. Chen, H. L. Chen, H. W. Sung, *ACS Nano* **2010**, *4*, 7467.
[85] C. Li, J. A. Xia, X. B. Wei, H. H. Yan, Z. Si, S. H. Ju, *Adv. Funct. Mater.* **2010**, *20*, 2222.
[86] K. J. Zhou, Y. G. Wang, X. N. Huang, K. Luby-Phelps, B. D. Sumer, J. M. Gao, *Angew. Chem., Int. Ed.* **2011**, *50*, 6109.
[87] X. P. Ma, Y. G. Wang, T. Zhao, Y. Li, L. C. Su, Z. H. Wang, G. Huang, B. D. Sumer, J. M. Gao, *J. Am. Chem. Soc.* **2014**, *136*, 11085.
[88] Y. G. Wang, K. J. Zhou, G. Huang, C. Hensley, X. N. Huang, X. P. Ma, T. Zhao, B. D. Sumer, R. J. Deberardinis, J. M. Gao, *Nat. Mater.* **2014**, *13*, 204.
[89] M. F. Kircher, L. Josephson, R. Weissleder, *Mol. Imaging* **2002**, *1*, 89.
[90] D. Tarin, B. J. Hoyt, D. J. Evans, R. C. Ydenberg, *Br. J. Cancer* **1982**, *46*, 475.
[91] L. A. Liotta, K. Tryggvason, S. Garbisa, I. Hart, C. M. Foltz, S. Shafie, *Nature* **1980**, *284*, 67.
[92] X. Lin, J. Xie, L. Zhu, S. Lee, G. Niu, Y. Ma, K. Kim, X. Y. Chen, *Angew. Chem., Int. Ed.* **2011**, *50*, 1569.
[93] S. Lee, E. J. Cha, K. Park, S. Y. Lee, J. K. Hong, I. C. Sun, S. Y. Kim, K. Choi, I. C. Kwon, K. Kim, C. H. Ahn, *Angew. Chem., Int. Ed.* **2008**, *47*, 2804.
[94] D. J. Ye, A. J. Shuhendler, L. N. Cui, L. Tong, S. S. Tee, G. Tikhomirov, D. W. Felsher, J. H. Rao, *Nat. Chem.* **2014**, *6*, 519.
[95] Y. Niko, Y. Arntz, Y. Mely, G. I. Konishi, A. S. Klymchenko, *Chem. - Eur. J.* **2014**, *20*, 16473.
[96] L. Liu, S. F. Wang, B. Z. Zhao, P. Pei, Y. Fan, X. M. Li, F. Zhang, *Angew. Chem. Int. Ed.* **2018**, *57*, 7518.
[97] M. Abaza, Y. A. Luqmani, *Expert Rev. Anticancer Ther.* **2013**, *13*, 1229.
[98] M. F. Ullah, A. Ahmad, S. H. Bhat, H. Y. Khan, H. Zubair, F. H. Sarkar, S. M. Hadi, *BioMetals* **2016**, *29*, 299.
[99] M. Gioia, G. F. Fasciglione, S. Monaco, R. Iundusi, D. Sbardella, S. Marini, U. Tarantino, M. Coletta, *J. Biol. Inorg. Chem.* **2010**, *15*, 1219.
[100] Y. Kato, C. A. Lambert, A. C. Colige, P. Mineur, A. Noel, F. Frankenne, J. M. Foidart, M. Baba, R. Hata, K. Miyazaki, M. Tsukuda, *J. Biol. Chem.* **2005**, *280*, 10938.
[101] Y. Kato, Y. Nakayama, M. Umeda, K. Miyazaki, *J. Biol. Chem.* **1992**, *267*, 11424.
[102] T. Matsubara, G. R. Diresta, S. Kakunaga, D. Li, J. H. Healey, *Front. Oncol.* **2013**, *3*, 199.
[103] X. Zhao, C. X. Yang, L. G. Chen, X. P. Yan, *Nat. Commun.* **2017**, *8*, 14998.
[104] J. Zhou, C. Fang, T. Chang, X. Liu, D. Shangguan, *J. Mater. Chem. B* **2013**, *1*, 661.
[105] D. Ni, W. Bu, E. B. Ehlerding, W. Cai, J. Shi, *Chem. Soc. Rev.* **2017**, *46*, 7438.
[106] H. B. Na, J. H. Lee, K. An, Y. I. Park, M. Park, I. S. Lee, D. H. Nam, S. T. Kim, S. H. Kim, S. W. Kim, K. H. Lim, K. S. Kim, S. O. Kim, T. Hyeon, *Angew. Chem., Int. Ed. Engl.* **2007**, *46*, 5397.
[107] T. Kim, E. J. Cho, Y. Chae, M. Kim, A. Oh, J. Jin, E. S. Lee, H. Baik, S. Haam, J. S. Suh, Y. M. Huh, K. Lee, *Angew. Chem., Int. Ed. Engl.* **2011**, *50*, 10589.
[108] G. S. Loving, S. Mukherjee, P. Caravan, *J. Am. Chem. Soc.* **2013**, *135*, 4620.
[109] C. Chu, H. Lin, H. Liu, X. Wang, J. Wang, P. Zhang, H. Gao, C. Huang, Y. Zeng, Y. Tan, G. Liu, X. Chen, *Adv. Mater.* **2017**, *29*, 1605928.
[110] L. Feng, Z. Dong, D. Tao, Y. Zhang, Z. Liu, *Natl. Sci. Rev.* **2017**, *5*, 269.
[111] J. Della Rocca, D. Liu, W. Lin, *Acc. Chem. Res.* **2011**, *44*, 957.
[112] G. Huang, K.-L. Zhang, S. Chen, S.-H. Li, L.-L. Wang, L.-P. Wang, R. Liu, J. Gao, H.-H. Yang, *J. Mater. Chem. B* **2017**, *5*, 3629.
[113] Y.-K. Peng, S. C. E. Tsang, P.-T. Chou, *Mater. Today* **2016**, *19*, 336.
[114] R. A. Schwendener, R. Wuthrich, S. Duewell, G. Westera, G. K. Vonschulthess, *Int. J. Pharm.* **1989**, *49*, 249.
[115] P. Mi, D. Kokuryo, H. Cabral, H. Wu, Y. Terada, T. Saga, I. Aoki, N. Nishiyama, K. Kataoka, *Nat. Nanotechnol.* **2016**, *11*, 724.
[116] Y. Chen, Q. Yin, X. Ji, S. Zhang, H. Chen, Y. Zheng, Y. Sun, H. Qu, Z. Wang, Y. Li, X. Wang, K. Zhang, L. Zhang, J. Shi, *Biomaterials* **2012**, *33*, 7126.
[117] Z. Ma, X. Jia, J. Bai, Y. Ruan, C. Wang, J. Li, M. Zhang, X. Jiang, *Adv. Funct. Mater.* **2017**, *27*, 1604258.
[118] J. J. Liu, Q. Chen, W. W. Zhu, X. Yi, Y. Yang, Z. L. Dong, Z. Liu, *Adv. Funct. Mater.* **2017**, *27*, 1605926.
[119] C. Kaittanis, T. M. Shaffer, A. Ogirala, S. Santra, J. M. Perez, G. Chiosis, Y. Li, L. Josephson, J. Grimm, *Nat. Commun.* **2014**, *5*, 3384.
[120] G. H. Gao, G. H. Im, M. S. Kim, J. W. Lee, J. Yang, H. Jeon, J. H. Lee, D. S. Lee, *Small* **2010**, *6*, 1201.
[121] G. H. Gao, J. W. Lee, M. K. Nguyen, G. H. Im, J. Yang, H. Heo, P. Jeon, T. G. Park, J. H. Lee, D. S. Lee, *J. Controlled Release* **2011**, *155*, 11.
[122] F. Fan, Y. Yu, F. Zhong, M. Gao, T. Sun, J. Liu, H. Zhang, H. Qian, W. Tao, X. Yang, *Theranostics* **2017**, *7*, 1290.
[123] L. Y. Wang, J. Huang, H. B. Chen, H. Wu, Y. L. Xu, Y. Li, H. Yi, Y. A. Wang, L. Yang, H. Mao, *ACS Nano* **2017**, *11*, 4582.
[124] X. H. Gao, Q. Yue, Z. N. Liu, M. J. Ke, X. Y. Zhou, S. H. Li, J. P. Zhang, R. Zhang, L. Chen, Y. Mao, C. Li, *Adv. Mater.* **2017**, *29*, 1603917.
[125] J. Gallo, N. Kamaly, I. Lavdas, E. Stevens, Q. D. Nguyen, M. Wylezinska-Arridge, E. O. Aboagye, N. J. Long, *Angew. Chem., Int. Ed.* **2014**, *53*, 9550.
[126] H. Zhou, J. Tang, J. Li, W. Li, Y. Liu, C. Chen, *Nanoscale* **2017**, *9*, 3040.
[127] J. Li, S. Wang, C. Wu, Y. Dai, P. Hou, C. Han, K. Xu, *Biosens. Bioelectron.* **2016**, *86*, 1047.
[128] J. S. Choi, S. Kim, D. Yoo, T. H. Shin, H. Kim, M. D. Gomes, S. H. Kim, A. Pines, J. Cheon, *Nat. Mater.* **2017**, *16*, 537.
[129] H. F. Zhang, K. Maslov, G. Stoica, L. V. Wang, *Nat. Biotechnol.* **2006**, *24*, 848.
[130] Q. Q. Miao, Y. Lyu, D. Ding, K. Y. Pu, *Adv. Mater.* **2016**, *28*, 3662.
[131] J. Jo, C. H. Lee, R. Kopelman, X. Wang, *Nat. Commun.* **2017**, *8*, 471.
[132] X. Z. Ai, C. J. H. Ho, J. Aw, A. B. E. Attia, J. Mu, Y. Wang, X. Y. Wang, Y. Wang, X. G. Liu, H. B. Chen, M. Y. Gao, X. Y. Chen, E. K. L. Yeow, G. Liu, M. Olivo, B. G. Xing, *Nat. Commun.* **2016**, *7*, 10432.